Title

Early detection of daylength variations with a feedforward circuit co-regulated by circadian rhythm and diel light-dark cycle

Authors

Nicholas Panchy[1,2], Albrecht G. von Arnim[1,3], Tian Hong[1,2,3]*

1. Department of Biochemistry & Cellular and Molecular Biology, The University of Tennessee, Knoxville, Tennessee, United States of America

2. National Institute for Mathematical and Biological Synthesis, Knoxville, Tennessee, United States of America

3. UT-ORNL Graduate School of Genome Science and Technology, The University of Tennessee, Knoxville, Tennessee, United States of America

* Corresponding author

E-mail: hongtian@utk.edu

Abstract

Light-entrained circadian clocks confer rhythmic dynamics of cellular and molecular activities to animals and plants. These intrinsic clocks allow stable anticipations to light-dark (diel) cycles. Many genes in the model plant *Arabidopsis thaliana* are regulated by diel cycles via pathways independent of the clock, suggesting that the integration of circadian and light signals is important for the fitness of plants. Previous studies of light-clock signal integrations have focused on moderate phase adjustment of the two signals. However, dynamical features of integrations across a broad range of phases remain elusive. We recently found that phosphorylation of RIBOSOMAL PROTEIN OF THE SMALL SUBUNIT 6 (RPS6 or eS6), a ubiquitous post-translational modification across kingdoms, is influenced by the circadian clock and the light-dark (diel) cycle in an opposite manner. In order to understand this striking phenomenon and its underlying information processing capabilities, we built a mathematical model for the eS6-P control circuit. We found that the dynamics of eS6-P can be explained by a feedforward circuit with inputs from both circadian and diel cycles. Furthermore, the early-day response of this circuit with dual rhythmic inputs is sensitive to the changes in daylength, including both transient and gradual changes observed in realistic light intervals across a year, due to weather and seasons. By analyzing published gene expression data, we found that the dynamics produced by the eS6-P control circuit can be observed in the expression profiles of a large number of genes. Our work provides mechanistic insights into the complex dynamics of a ribosomal protein, and it proposes a previously underappreciated function of the circadian clock which not only prepares organisms for normal diel cycles but also helps to detect both transient and seasonal changes with a predictive power.

Author summary

Circadian clocks provide animals and plants with internal rhythmic dynamics that anticipate light-dark cycles in a consistent fashion. Many genes in plants are controlled by both the circadian clock and light-dark cycles through independent pathways. One paradigm for the interaction between clock and light signaling pathways is expressed in the 'external coincidence' model, which explains the seasonal flowering of plants in response to daylength. However, it is unclear how many different such paradigms can be encoded in the light-and-clock signaling network. Based on a recent observation that circadian rhythms and light-dark cycles drive the phosphorylation of ribosomal protein eS6 with opposing phases, we built a mathematical model for the eS6 phosphorylation (eS6-P). We found that these observations can be explained by a feedforward circuit describing a clock-independent light pathway and a clock-dependent pathway that influences eS6-P dynamics across the day. This circuit has the remarkable feature of detecting the daylength variations at the beginning of a day by integrating the signals from the clock and the light-dark cycles in a phase-sensitive manner. We used realistic photoperiod data to show that the circuit can detect both transient (weather) and long-term (seasonal) changes in daylength variations. These results show rich dynamic information from clock-light signal integration and suggest a new property of the circadian clock in robustly detecting changes in light conditions.

Introduction

Circadian clocks provide animals, plants and certain microbes with rhythmic dynamics. These circadian pacemakers confer fitness advantages to the organisms by establishing stable anticipation of diel light-dark cycles [1,2] as well as regulating broad morphological changes over the course of the year [3]. In the plant model organism *Arabidopsis thaliana (A. thaliana)*, the circadian clock consists of at least four interacting gene modules that form negative feedback loops, which govern an intrinsic oscillator [4,5]. The expression dynamics of several hundred genes in *A. thaliana* are controlled by this circadian oscillator [6,7]. The circadian oscillator retains its essential dynamical features under constant light conditions, reflecting its intrinsic nature [8], but the phase of the oscillations can be adjusted in a process called entrainment by the lights-on signal at dawn [5,9]. In addition, however, the light-dark cycle regulates a large number of genes in a clock-independent fashion [8,10]. Therefore, molecular activities in plants are influenced by at least two periodic signals. Previous studies have found that cellular activities in *A. thaliana*, such as the abundance of the regulator of flowering time CONSTANS (CO) and the cytosolic calcium concentration, require signals from both the clock and the light-dark cycle to regulate timing (i.e. the phase of peak activity) [8,9,11]. For example, for many mRNA transcripts, the circadian clock leads to a moderate phase shift in the onset or peak time as compared to the light cycle alone [8,9,11]. However, these paradigms only represent *one* of the many diverse co-regulation modes of clock-light signal integration. It remains unclear whether the integration of circadian and diel light-dark cycles underpins other paradigms of signal processing.

The phosphorylation of RIBOSOMAL PROTEIN OF THE SMALL SUBUNIT 6 (RPS6 or eS6) is a post-translational modification that occurs in a wide range of organisms including animals and plants [12-14]. Mice that have only a non-phosphorylatable eS6 show abnormalities at the organismal level (e.g. muscle weakness), indicating that this modification is functionally significant [15]. However, while it has been suggested that the eS6 phosphorylation (eS6-P) is implicated in ribosome biogenesis in mammals [12], its

77 biochemical consequence and specific activity, including its molecular role in *A. thaliana*, are largely
78 unknown [13]. Interestingly, eS6-P is widely used as a bioreporter for the activity of Target Of Rapamycin
79 (TOR) kinase, a central controller of cell growth and aging [16,17]. We recently found that eS6-P in *A.*
80 *thaliana* is co-regulated by both the circadian clock and the diel cycle, as eS6-P exhibits cycling behavior
81 both in a severely clock-deficient strain and under constant light conditions [18]. Unlike other extensively
82 studied cellular processes, eS6-P is controlled by the clock and light-dark cycles in a strikingly opposite
83 manner: in the wild-type strain under constant light the circadian clock drives eS6-P with a peak during
84 the subjective night, whereas in a clock-deficient strain the diel light-dark cycle drives eS6 with a peak
85 during the day [18,19]. However, the biological significance of this remarkable phenomenon at cellular
86 and organismal levels remains elusive.

87 In this study, we constructed a mathematical model to examine the signaling network that regulates eS6-
88 P in *A. thaliana*. We calibrated the model with experimental measurements of the circadian clock and eS6-
89 P under various conditions. We found that the key dynamics of eS6-P can be explained by a feedforward
90 loop that connects the periodic light signals to eS6-P with a direct arm and an indirect arm via the circadian
91 clock. Although this feedforward loop is largely incoherent at the steady state of a symmetrical light-dark
92 cycle (12-hour-light and 12-hour-dark), the amplitude of its output exhibits a high sensitivity to variations
93 in daylength, due to the interaction between the two cyclic components in the loop. Notably, we found a
94 characteristic early day peak of eS6-P that detects and anticipates long days. Furthermore, we combined
95 the model with realistic photoperiod data containing both transient perturbations and long-term
96 variations of light-dark cycles and demonstrated that the detection of daylength variations by this circuit
97 communicates information about changes of both the season and the local environment throughout the
98 year. By comparing our model with several representative competing models with various circuits
99 transmitting only light signals, we found that the robust detection of day length variations requires both
100 the circadian clock and the clock-independent light sensor. Our work demonstrates a remarkable

information processing capacity of a feedforward loop that integrates circadian and light-dark cycles, and it reveals a previously underappreciated role of the circadian clock in anticipating and predicting the changes in light conditions rather than the stable photoperiod.

Results

A mechanistic mathematical model characterizes dynamical features of a feedforward loop controlling eS6-P

To gain a better understanding of the mechanisms underlying the dynamics of eS6-P, we built a mathematical model that includes a light-entrained circadian clock and a light-dependent, clock-independent signaling pathway that regulates the phosphorylation of eS6 (Fig 1A). The latter light-pathway consists of TOR, a kinase that transmits light signals, and ribosomal S6 kinase (S6K), a substrate of TOR [20-23]. S6K has been shown to phosphorylate eS6, and the TOR-S6K axis is known as a primary pathway for eS6-P in multiple organisms including plants [17]. The clock component of the model is described by four interacting components (LHY/CCA1, the evening complex (EC), PRR9/PRR7, and PRR5/PRR1, denoted as C1, C2, C3 and C4 respectively in this study). It contains the core repressilator of the plant circadian circuit and has previously been used to model the circadian clock (Fig 1A) [4,24-26]. We used this model to capture the essential dynamical features of the clock rather than the molecular details, so we focused on this four-component core repressilator and neglected the additional feedbacks in the clock [4]. Because we previously observed that eS6-P oscillates under constant light [18], we also considered clock-driven regulation of eS6 phosphorylation and dephosphorylation in our model (Fig. 1A). Before parameter estimation, each clock component in the model was assumed to regulate (activate or inhibit) the phosphorylation or dephosphorylation of eS6 with unknown parameters. Because we assumed that the clock does not receive signals from the clock-independent pathway or eS6, we first

obtained a parameter set for the clock component by fitting the clock model using a qualitative objective function to capture the basic behaviors including cyclic variation in response to light-dark cycles (entrainment) and cycling under constant light conditions (see Methods, Fig. S1). We then compared the simulated clock gene dynamics to previously published expression data [27] to ensure that the model properly represents the phase and shape of the time course measurements (Fig. S2).

Fig. 1. Network structure of the eS6-P regulatory circuit and comparisons between simulations and experiments. (A) An influence diagram of a model of the light and clock driven feedforward regulatory system that regulates eS6-P (Clock+Light Model). This model consists of two cycling systems: the light-dark cycle (an oscillatory input) and the circadian clock (an autonomous oscillator). Each cycle regulates cellular processes independently. The regulation by light-dark cycle is mediated by TOR-S6K pathway, and the clock driven regulation is mediated by transcription factors belonging to the LHY/CCA1 (C1), Evening Complex (EC,C2), PRR9/7 (C3), PRR5/1 (C4) modules which contain a repressilator circuit and additional interactions. The light-dark cycle also regulates the circadian clock via the LHY/CCA1 and PRR9/7 modules (entrainment), thus creating a feedforward circuit. Arrows with circle head show influence of unknown directions (positive or negative) before parameter estimation. **(B)** Model predictions (black) and experimental observations (red) of eS6-P under wild-type in long-days (16:8, LD). Error bars indicate standard deviation of pooled measurements at various circadian times. Circadian time is relative to dawn, and regions shaded with grey indicate period of darkness. Blue dots show the raw data points collected prior to pooling over a period of 84 hours [18]. **(C)** Model predictions (black) and experimental observations (red) of eS6-P under long-days (16:8, LD) but with a deficient clock (CCA1-overexpression). Error bars indicate standard deviation of pooled measurements at various circadian times. Time is measured and the graph is shaded as in **(B)**. **(D)** Model predictions (black) and experimental observations (red) of eS6-P under constant light. Error bars indicates standard deviation of pooled measurements at

148 various circadian times. Circadian time is measured relative to subjective dawn (Zeitgeber time, ZT) and
149 regions shaded grey indicate periods of subjective night. eS6-P is shown in arbitrary units (a. u.) (see
150 Methods). **(E)** An influence diagram of our model of eS6-P updated with the direction (triangle arrowhead:
151 activation, flat arrowhead: repression). Note that the ambiguous (diamond) regulation of the clock by light
152 reflects that light regulates LHY/CCA1 and PRR9/PRR7 in opposite directions (we assume that light
153 represses CCA1 stability [49], which is important to restrict the LHY/CCA1 peak to dawn). **(F)** An overlay
154 of clock element activities on top of the eS6-P trajectory in wild type under a long-day cycle. The eS6-P
155 cycle is indicated by the solid black curve and the clock components are represented by colored curves
156 (red = C1 = LHY/CCA1, blue = C2 = EC, orange = C3 = PRR9/PRR7 , green = C4 = PRR5/PRR1). Circadian time
157 is measured relative to dawn.

158

159 Next, we fit the Clock+Light model that contains both clock-dependent and clock-independent pathways
160 regulating eS6-P to our recent measurement of eS6-P dynamics under three experimental conditions: a
161 wild-type (WT) strain under long day (LD, 16-hour-light and 8-hour-dark) condition, the WT strain under
162 constant light (LL) condition, and a clock-deficient strain under LD condition (CCA1-overexpression) [18].
163 Using an evolutionary algorithm with a likelihood-based objective function, we found optimized
164 parameter sets that produced trajectories that reasonably matched the experimental data in all three
165 conditions (Fig. 1B-D). Importantly, the model captured the remarkable dynamical features of eS6-P: light
166 alone drives the upregulation of eS6-P during the day (Fig. 1C) whereas the clock alone drives the
167 upregulation of eS6-P during the subjective night (Fig. 1D). Our model also recapitulated the day-peak of
168 the eS6-P when both clock and light-dark cycles are present, suggesting the dominant role of the light-
169 dark cycle. Furthermore, the model predicted a peak of eS6-P shortly after dawn that was not measured
170 experimentally. We found that this observation was not due to the choice of a particular parameter set:
171 the majority of the top 70 (or 5%) models (based on likelihood) from multiple optimization runs generated

the same behavior (Fig. S3A). Conversely, the next 70 models lacked the dawn peak, but those models also lacked oscillations under constant light, suggesting a loss of clock regulation (Fig. S3B). Our subsequent analyses are based on the top performing model, which produced a moderate peak of eS6-P after dawn.

We next examined how the clock and the light-dark cycles influenced eS6-P mechanistically. While the clock-independent pathway had an obvious mechanism of action, in which the light signal activates a cascade of two kinases that give rise to eS6 phosphorylation, the clock pathway involved a nontrivial combination of molecular influences. We found that eS6-P is regulated by multiple clock-genes that peak at different time points during the day (Fig 1E). Specifically, LHY/CCA1 and PRR9/PRR7 both regulated eS6 during the early day with different phases of activity (LHY/CCA1 at dawn and PRR9/PRR7 a few hours after dawn) and opposite effects on eS6 dephosphorylation (LHY/CCA1 inhibits and PRR9/PRR7 promotes dephosphorylation). In contrast, while EC and PRR5/PRR1 also have opposing influences, their activities largely overlapped and canceled each other out. These clock influences collectively resulted in the stably high amount of eS6-P between the early day and dusk, while the early day peak resulted from a coincidence of light, the peak LHY/CCA1 activity, and the absence of peak PRR9/PRR7 activity (Fig 1F). As such, our model showed that at the steady state under LD, the circadian clock and the light-dark cycle influenced eS6-P in a generally opposing manner: during the day, eS6-P is promoted by light but inhibited by PRRs, while during the night, the anticipatory rise of LHY/CCA1 promoted eS6-P prior to dawn, leading both to rapid early rise and the early day peak under normal LD conditions, and the shift in the rise into the subjective night under constant light. Considering the clock's dynamics are light-entrained, the resulting model behaved as a feedforward loop that is largely incoherent at steady state.

In conclusion, our calibrated model captured the observed dynamics of eS6-P under multiple conditions, and allowed us to make predictions about the mechanisms underlying these intriguing dynamics. Note that although our discussion primarily focuses on one optimized model, we have reproduced our key

196 conclusions with distributions of parameters rather than a single parameter set (Fig. S3), and with a much
197 more detailed clock model which includes both mRNA and protein concentrations (Fig. S4) [4].

198

199 **Integration of circadian clock and light-sensing pathways detects and anticipates long daylength upon**
200 **transient perturbations of light-dark cycles**

201 We next focused on the dynamics of eS6-P after dawn, when the coincidence of clock and light signals
202 gave rise to a sharp rise and a peak in the model (Fig. 1B-D). We hypothesized that at this key time interval
203 a change in the phase of the lights-on signal significantly affect the dynamics of the model output because
204 the distinct influences of light and clock can synergize with each other depending on their relative phase.
205 We therefore focused on variations in the timing of the transition from night to day (t_{ND}), as they might
206 be used as proxies for transient changes in the local environment (such as weather)or long-term seasonal
207 changes. We ran simulations with the optimized Clock+Light model (Fig. 1E) under the 12-hour-light and
208 12-hour-dark (12L:12D) condition. After the system reached steady state (Day 0), we varied t_{ND} (+/- 4
209 hours) at the start of a single day (Day 1), and tracked the trajectories of eS6-P from the perturbed day
210 and onwards (Fig. 2A). We found that the transient variation of t_{ND} resulted in significant changes in the
211 abundance of eS6-P (response) in the early day, but the responses converged as the day continued. In
212 particular, an early night-to-day transition time ($t_{ND}<0$) gave rise to a higher response including an early
213 day peak, as previously observed with the base model under LD condition (Fig. 1B, Fig. 2B purple), whereas
214 a late transition time ($t_{ND}>0$) had the opposite effect and resulted in a trough (Fig. 2B yellow). In addition,
215 early day maximum eS6-P (defined as the maximum eS6-P over the 4 hours after dawn) varied by as much
216 as 13.8% relative to the case of $\Delta t_{ND} = 0$. We found that the early day peaks (transient responses that are
217 greater than the steady-state response during the day) appeared only when the daylength exceeded 12

hours (Fig. 2B cyan). These results show that the eS6-P control circuit detected phase variations of the lights-on signal and thus effectively sensed daylength variation at the beginning of the day.

Fig. 2. Response of eS6-P to variations of the night-to-day transition time. (A) Diagram of perturbations of the night-to-day transition and the effect of daylength relative to a 12-hour-light-12-hour-dark (12L:12D) day. The unperturbed ($\Delta t_{ND} = 0$) and perturbed (Δt_{ND} +/- 4 hours) days are labeled. The day period is shown by yellow shaded regions and the maximum extent of the change in daylength is shown by differential shading. The system reached steady state before Day 0. **(B)** Trajectories of eS6-P in response to variations of the night-to-day transition time from $\Delta t_{ND} = -4$ (purple) to $\Delta t_{ND} = 4$ (yellow) in 0.5-hour increments. All trajectories start at the dusk of the previous day (Day 0, unperturbed), and end at the dusk of the current day (Day 1, perturbed). Dotted lines show trajectories in the absence of light. Thick solid curves show trajectories in the early day (first four hours after dawn), and thin solid curves show trajectories in the remaining hours of the day. Short line segments at the bottom show the time of dawn for each trajectory. **(C)** Side by side plots of clock perturbations in response to varying night to day transition and the resulting effects on eS6-P. For simplicity, we only show the $\Delta t_{ND} = -4$ (purple), $\Delta t_{ND} = 0$ (red), $\Delta t_{ND} = 4$ (yellow) in the bottom figure. In the top panel, color indicates clock factor (red = C1 = LHY/CCA1, blue = C2 = EC, orange = C3 = PRR9/PRR7, green = C4 = PRR5/PRR1), while shade of color represents the timing of dawn (dashed, $\Delta t_{ND} = -4$; regular solid, $\Delta t_{ND} = 0$; semitransparent solid, $\Delta t_{ND} = 4$). Dashed lines show the corresponding times while circles on the clock factors' curves highlight how the ratio between LHY/CCA1 and PRR9/PRR7 corresponds to peak height of the response. In all panels, Circadian time is shown in hours relative to normal time of dawn (i.e. +/- 0 hours).

We found that the sensitivity of eS6-P to changes in the light-dark cycle was associated with the altered relative phase of clock-gene activities with respect to the dawn (Fig. 2C, gray lines) upon perturbations of the light-dark cycle. For example, the earlier dawn allowed synergy between light signal, peak of CCA1/LHY and relatively low activities of PRR modules to give rise to a strong eS6-P response (Fig. 2C). This change of relative phase occurred despite the influence of the transient phase shift on the clock gene dynamics as a form of entrainment (Fig. 2C upper panel). Variation in photoperiod length has been previously shown to affect the absolute phase of circadian genes, altering both their timing relative to dawn and the intervals between peak expression of different circadian genes, with the gap between CCA1/LHY and PRR9 growing as the photoperiod becomes longer [26,28]. These results suggest that the circadian clock plays an essential role in the regulation of eS6-P, particularly with regard to its early day dynamics.

We therefore asked whether the circadian clock is required for the eS6-P circuit (Fig. 1E, Clock+Light model) to detect long daylength with an early day peak. To this end, we constructed three alternative models that describe various modes in which eS6-P may respond to the light signal in the absence of the clock (Fig. 3A, see Table S2 for parameters). These models are: 1) a linear circuit that transmits light signals to eS6-P (Fig. 3A, top panel), 2) an incoherent feedforward loop (IFFL) that produces an early day peak similar to what the Clock+Light model does under LD condition (Fig. 3A and B, middle panels), and 3) a coherent feedforward loop (CFFL) that allows slow decline of eS6-P upon the withdrawal of light signals (Fig. 3A, lower panel). Note that none of these three models were able to fully fit the observed data (e.g. Fig. 1D) due to the lack of clock regulation. Rather than evaluating these models in terms of their fit to data, we focused on their performance in terms of detecting daylength variations upon dawn.

Fig. 3. Response of alternative models of eS6-P circuit to variations of the night to day transition time. **(A)** Influence diagrams of the three alternative models of eS6-P circuit. In each diagram, the regulatory

263 factors are indicated by the lettered black circles, and regulatory interactions are denoted by colored lines
264 (blue = activation, red = repression). Right panels show simulation trajectories with these models under
265 the LD condition. Gray regions show the period of night. **(B)** Trajectories of eS6-P in response to variations
266 of the night to day transition time from Δt_{ND} = -4 (purple) to Δt_{ND} = 4 (yellow) in 0.5-hour increments. All
267 trajectories start at the dusk of the previous day (Day 0, unperturbed), and end at the dusk of the current
268 day (Day 1, perturbed). Dotted lines show trajectories in the absence of light. Thick solid curves show
269 trajectories in the early day (first four hours after dawn), and thin solid curves show trajectories in the
270 remaining hours of the day. Short line segments at the bottom show the time of dawn for each trajectory.
271 **(C)** Left: peak metric (ratio of the early day maximum of eS6-P to the eS6-P levels at the dusk) with respect
272 to the perturbations of the daylength. Right: activation time of the eS6-P after dawn with respect to the
273 perturbations of the daylength. Activation time is defined as the time for eS6-P to reach $x_0 + 0.9(x_s -$
274 $x_0)$, where x_0 is the eS6-P level at the dawn and x_s is the eS6-P level at the dusk.

275

276 Each of the three alternative models generated a constant level of eS6-P upon the perturbations of
277 daylength (Fig. 3B cyan). Particularly, the early day peak produced by the IFFL model did not distinguish
278 short and long daylengths (Fig. 3B middle). This insensitivity to daylength variations with the alternative
279 models was reflected in the stable maximum early responses of eS6-P regardless of their ratios to steady
280 state (or end-of-day) eS6-P levels (Fig. 3C left). In addition, we found that the daylength-sensitive early
281 response with the Clock+Light model was anticorrelated with the time for eS6-P to reach its steady state
282 level, e.g. an early dawn accelerated the response of eS6-P (Fig. 3C right). These results suggest that
283 detection of long daylength with early day peaks is a feature that requires the integration of the circadian
284 clock and the clock-independent light-sensing pathway.

285 Because realistic perturbations of daylength may occur through changes of light conditions at both dusk
286 and dawn and on multiple days, we next considered the effects of multiple variations in our simulations.
287 We first allowed -/+ 2 hours of variation in t_{ND} followed by +/-2 hours of variation in the day-to-night
288 transition (t_{DN}) during dusk the previous day (Fig. 4A). Perturbations in each t_{DN}-t_{ND} pair acted in the same
289 direction to either lengthen or shorten the intervening night (Fig. 4A and B, vertical lines). With the
290 Clock+Light model, we found that consecutive changes in dusk and dawn timing gave rise to significant
291 variability in eS6-P response, similar to what was obtained with -/+ 4 hours of t_{ND} alone (Fig. 2B, Fig. 4B
292 and C). Interestingly, +/- 2 hours perturbations of t_{ND} or t_{DN} alone did not generate an early day peak (Fig.
293 4B and C). This suggests that changes in the timing of dusk can be integrated into the eS6-P response by
294 the Clock+Light circuit after dawn and serve as a predicting factor for the current daylength. The
295 incorporation of information in the previous day shows that the Clock+Light circuit can anticipate the
296 daylength changes with a memory capacity.

297 We next examined the effect of changes to t_{ND} on two consecutive days. We observed a slightly increased
298 dynamic range of early eS6-P peak on the second early day compared to the first day with the Clock+Light
299 model (Fig. S5). These results indicate that the Clock+Light circuit was able to detect changes in daylength
300 beyond the altered timing of the current dawn.

301

302 **Fig. 4. Response of eS6-P to variations in night to day transition time following changes of day to night**
303 **transition time the previous dusk. (A)** Diagram of perturbations of the day to night transition and the
304 night to day transition on two consecutive days. The first (perturbed at dusk, Δt_{ND} = -/+ 2 hours) and
305 second days (perturbed at dawn, Δt_{ND} = +/- 2 hours) are labeled. The day period with light is shown by
306 yellow shaded regions and the maximum extent of the change in daylength is shown by differential
307 shading. **(B)** Trajectories of eS6-P in response to variations of the day to night transition time and/or the

night to day transition time from Δt_{ND} = -2, Δt_{DN} = 2 (purple) to Δt_{ND} = 2, Δt_{DN} = -2 (yellow) in 0.25-hour increments. Short line segments at the bottom show the time of dawn or dusk for each trajectory. Upper: dawn perturbation only. Middle: dusk perturbation only. Bottom: both perturbations. **(C)** Peak metric (ratio of the early day (Day 1) maximum of eS6-P to the eS6-P levels at the dusk) with respect to the perturbations of the daylength under various perturbation scenarios.

Integration of circadian clock and light-sensing pathway detects gradual variations of light-dark cycles

We next asked whether the eS6-P circuit responds to progressive, long-term variations of the light-dark cycle, reflective of seasonal changes in the cycle throughout a year. We used a Solar Calculator provided by the National Oceanic and Atmospheric Administration (NOAA) to generate a data set of 'ideal' (i.e. unaffected by transient local changes) daylengths over the course of a year. We simulated the Clock+Light model based on these light-dark cycles for one year at two locations representing the extreme latitudes of the *A. thaliana* distribution, Oslo, Norway, and Praia, Cape Verde [29]. As expected from the analysis of transient changes in dawn timing, our model showed a sensitivity of eS6-P to changes in daylength over the year (Fig. 5). The range of eS6-P was correlated with the degree of variation in daylength, which was broader in Oslo (6.2 to 19.0 hours, Fig. 5A) compared to Praia (11.3 to 13.0 hours, Fig. 5B). We observed variations in both the early-day maximum and early-day minimum levels of eS6-P in Oslo (Fig. 5A, orange and pink), with the early-day maxima increasing dramatically as daylength approached its yearly maximum in the summer. Starting from Day 89 of the year, the early-day maxima increased until it reached 148% of the daily steady state at Day 170. As such, we conclude that changes in the daylength over a year are able to the variations in the early-day peak of eS6-P, with the early day maxima exceeding the daily steady state level around 13.5 hours of light. In contrast, much smaller variations of the early-day eS6-P, which never exceeded the daily steady state levels, were observed with the yearly light-dark

cycle data in Praia (Fig. 5B), which has a maximum daylength of 13.0 hours. These results suggest that the eS6-P circuit can detect seasonal changes of the light-dark cycles by varying the magnitude of the responses after the dawn and thus is sensitive to changes in daylength even when they occur gradually.

Fig. 5. Simulated amounts of eS6-P in response to seasonal changes in daylength over a year. (A) Simulation of eS6-P over a full year using daylength data for Oslo, Norway (the NOAA Solar Calculator). The left figure shows the eS6-P time course over the full year (gray), overlaid with the early-day maximum (green), early-day minimum (pink), and daily steady state (end-of-day, or dusk) level (black). Peak metric (orange) is defined as the ratio of early-day maximum to the daily steady state level. The right figure shows the eS6-P profiles of individual days selected every two weeks from Day 7 to Day 175 of the year. Time 0 is the actual dawn of each day. The color of each curve corresponds to the week number and is correlated with the daylength from short (yellow) to long (purple). Triangles indicate the time at which the end-of-day eS6-P level was measured, and blue dots indicate the position of the early-day peak. **(B)** Simulation of eS6-P across a full year using daylength data for Praia, Cape Verde (the NOAA Solar Calculator). Upper and lower figures are as described in **(A)**. The globe on the left of each panel shows the latitude of the position that the daylength was simulated for.

We next asked whether the eS6-P circuit can detect changes in light-dark cycles due to transient changes (such as weather) as well as seasonal changes. We obtained a year-long environmental radiometry data from Harvard Forest [30]. We normalized the measurement of downward photosynthetic radiation based on the ideal daylength calculations for Boston, Massachusetts from NOAA and obtained a time-series data of realistic light-dark cycles over a year (see Methods). Briefly, a threshold value was used to define day/night with the Harvard Forest data, and the value was chosen to minimize the mean difference

between the inferred hours of daylight and NOAA estimations of daylength. We compared the simulation results for idealized and observed daylength data (Fig. 6) With the idealized daylengths in Boston (9.4 to 15.4 hours), we observed moderate early day peaks in the middle of the year (Fig. 6A). However, transient changes in the observed light data resulted in changes in daylength of up to 1.5 hours, which in turn gave rise to significant variation of early-day peak of eS6-P in response to the changes of sunlight due to daily weather in addition to seasonal changes of sunlight (Fig. 6B). Although transient changes mainly reduced the daylengths from the idealized day lengths throughout the year, there is a significant difference in terms of peak metric between longer (>13 hours) and shorter (<13 hours) days based on the realistic sunlight data (1.01 vs. 0.96. Welch's t-test, $p = 2.7\times10^{-34}$). Furthermore, the absolute difference in early-day peak between idealized and realistic days was greater during longer days (> 13 hours) than during shorter days (< 13 hours) by 10-fold (Welch's t-test, $p = 7.5\times10^{-32}$). As such, these weather induced changes primarily exist in long days, during which the early response of eS6-P is most sensitive to daylength changes. To further illustrate this point, we compared in simulated early day peaks between idealized and realistic days: in both simulations the peak to steady state ratio remained low during short days and increased around a daylength of 13 hours, but the ratios of the two simulations diverged as days grew longer (Fig. 6C). Together, these results show that the eS6-P circuit can detect variations in light-dark cycles when both seasonal and local, transient (weather) changes are considered.

Fig. 6. Simulated amounts of eS6-P in response to transient and seasonal changes in daylength over a year. (A) Simulation of eS6-P across a full year using daylength data for Boston, Massachusetts (the NOAA Solar Calculator). The left figure shows the eS6-P time course over the full year (grey), overlaid with the early-day maximum (green), early-day minimum (pink), and daily steady state (end-of-day, or dusk) level (black). Peak metric (orange) is defined as the ratio of early-day maximum to the daily steady state level. The right figure shows the eS6-P profiles of individual days selected every two weeks from Day 7 to Day

175 of the year. Time 0 is the actual dawn of each day. The color of each curve corresponds to the week number and is correlated with the daylength from short (yellow) to long (purple). Triangles indicate the time at which the end-of-day eS6-P level was measured, and blue dots indicate the position of the early-day peak. **(B)** Simulation of eS6-P over a year using the full year daylength data derived from Harvard Forest radiometry data [26]. The eS6-P time course over the full year (grey) is overlaid with the early-day maximum (green), early-day minimum (pink), and daily steady state (end-of-day, or dusk) level (black). Peak metric (orange) is defined as the ratio of early-day maximum to the daily steady state level. **(C)** The average peak metric (ratio of the early day maximum of eS6-P to the eS6-P levels at the dusk) for NOAA (open circle) and Harvard Forest (closed circle) days binned according to their realistic daylength (every half hour from 8 to 15 hours). Error bars indicate the standard deviation of Harvard Forest days in each bin. The color of the points and bars is correlated with daylength from short (yellow) to long (purple). The globe on the left shows the latitude of the position that the daylength was simulated for.

The sensitivity of early eS6-P responses to daylength variations raises a question whether this detection of daylength variation is robust with respect to fluctuations of light conditions due to, for example, temporary shading by taller plants, and well as fluctuations in molecular concentrations. We therefore introduced high frequency white noise to the variables describing either the amount of transmitted light or eS6-P itself. We used mutual information to quantify the signal transmitted from varied daylength to the early eS6-P response. We found that more than 50% of the mutual information (compared to the noise-free condition with a finite number of bins) was retained (>1 bit) in the presence of significant fluctuations of light or eS6-P (amplitude parameter $\mu = 5$, or about 23% coefficient of variation in light signal) (Fig. S6). This result suggests that the system is robust with respect to the rapid fluctuations of light or molecular concentrations, while it maintains its capacity to detect daylength variations. Intuitively, the peak of eS6-P in long days is driven by a clock-based, slowly increasing trajectory starting from night, and

this slow dynamics serves as a signal integration, or averaging method, to reduce the effect of high frequency noise.

Dynamical features of the eS6-P circuit represent expression profiles of a large number of genes

Because many genes in *A. thaliana* are co-regulated by the circadian clock and light-dark cycles, we hypothesized that the dynamic features of eS6-P can be observed in the expression patterns of other genes. To identify genes whose expression may resemble the profile of eS6-P, we reanalyzed an *A. thaliana* cyclic gene expression data set reported by Dalchau et al. [8], which is based on previously published microarray data with expression patterns of *A. thaliana* genes under LD and LL conditions [6,31,32]. By calculating the phase shift of the peak expression between measurements under LD and LL conditions, we identified 126 genes where peak expression appears in the early day under LD (0-6 hours after dawn) and regressed into the night under LL condition (18-24 hours after dawn), emulating the clock driven sensitivity that we observed in our eS6-P model and the underlying experimental data (see Methods). We next reanalyzed our previously published RNA sequencing data for *A. thaliana* genes under clock-deficient condition (CCA1 overexpression) [10], and further refined the list of 126 genes by selecting those that have peak expression during the day and have significantly higher expression during the day than during the night under the clock-deficient condition (see Methods). With these selection criteria based on the two data sets (Dalchau et al. and Missra et al. [8,10]), we have identified 92 genes of which time course expression profiles are similar to that of eS6-P (Table S3). As expected, genes identified in this manner exhibited expression patterns qualitatively similar to eS6-P dynamics (Fig. 7).

Fig. 7. Genes in *A. thaliana* with eS6-P like expression patterns. (A) The distribution of the peak phase shift between LD and LL conditions for 92 genes for which phases of expression profiles are similar to

425 those of eS6-P (blue). Equivalent phase shifts for all cyclic genes in the list generated by Dalchau et al. [8]
426 are in gray. **(B-D)** The mRNA expression patterns of 92 genes with phases of expression profiles similar to
427 those of eS6-P for wildtype under LD (B), wildtype under LL (C) and CCA1-overexpression under LD (D)
428 conditions. Time course expression profiles of individual genes are shown as colored curves while the solid
429 black line shows the average expression of all 92 genes. The dotted black line is the average expression
430 pattern of all cyclic genes in the list generated by Dalchau et al. [8]. Expression values in all panels were
431 normalized from 0 to 1, such that 0 corresponds to the minimum and 1 correspond to the maximum for
432 each individual gene. **(E)** Distributions of the difference in average mRNA expression level between day
433 and night of 92 eS6-P like genes (blue) and all cyclic genes in the list generated by Dalchau et al. [8] (gray)
434 under CCA1 overexpression condition. Positive values indicate greater average expression during the day
435 and negative values indicate greater average expression during the night.

436

437 Dalchau et al. [8] classified genes with cyclic expression patterns into three categories based on whether
438 the clock or the light-dark cycle dominates the amplitude of the oscillation in mRNA levels: clock-dominant,
439 light-dominant and co-regulated. Note that all three types of genes can be influenced by both the clock
440 and the light-dark cycles, and the category 'co-regulated' here has a more stringent definition in terms of
441 the amplitudes (see Methods). Not surprisingly, the time course profile of eS6-P is categorized as 'co-
442 regulated' based on the definition of Dalchau et al. (see Methods). We found that out of the 92 eS6-P like
443 genes, 66 are classified as 'clock-dominant', while 25 are 'co-regulated' and only 1 is 'light-dominant',
444 suggesting the clock plays a prime role in generating this pattern of expression.

445 We next performed gene ontology (GO) enrichment analysis with the 92 eS6-P like genes using the set of
446 all annotated genes in *A. thaliana* as a background. We found that eS6-P like genes genes are enriched for
447 light response, photosynthetic regulation, and chloroplast localization, as expected from their

448 responsiveness to light (Table S4). Many of the same biological process and cellular compartment terms
449 are also enriched amongst the set of all genes that show cyclic expression patterns (Table S5). However,
450 the enrichment of specific molecular functions regarding memebrane transport (zinc, ferrous iron, and
451 protons) and activities (ATPpase and thioredoxin-disulfide reductase) is unique to eS6-like genes,
452 suggesting they represent a more specialized subset of the light-clock regulated genes. Overall, this
453 suggests that eS6-P like behavior, a photoperiod sensitive shift in peak activity around dawn, is associated
454 with specific light-dependent metabolic functions.

455 These results suggest that the dynamics of eS6-P may represent a broad range of transcriptional, post-
456 transcriptional and post-translational activities in *A. thaliana,* particularly in association with light driven
457 and responsive metabolic functions. While eS6-P is co-regulated by both the light and clock, the phase
458 variation in our model is driven by the clock, and this is consistent with the observation that this pattern
459 is associated with many clock-dominant genes. The similarity of dynamical features among these cellular
460 activities does not indicate a causal relationship, but it raises the possibility that the daylength detection
461 and anticipation features of such dynamics may be used by a large system of molecules in *A. thaliana*. This
462 suggests that the cyclic phosphorylation of eS6 may serve as a key signaling factor or an effector
463 integrating ribosomes into this detection and anticipation system.

Discussion

Robustness and sensitivity of the clock with respect to light conditions

In this study, we built a mathematical model that describes the dynamics of eS6-P, a ribosomal post-translational modification that occurs in many eukaryotic species. A feedforward regulatory loop connects light signals to eS6-P through a clock dependent pathway and a clock independent pathway. We found that the response of eS6-P is sensitive to the changes of the light-dark cycles, e.g. the daylength variations that are reflected in the time of the dawn. The circuit therefore enables cells to detect and anticipate such variations which may result from changes in season and/or transient changes in weather. We showed that the circadian clock plays important roles in this information processing function. This feature is different from the well-known function of the clock, which ensures robust anticipation of light-dark cycles even under fluctuating light conditions [33,34]. Our study shows that the clock can be used to robustly detect the variations of light conditions at the beginning of a day, which is a function in addition to its traditional role in generating stable rhythmic cues that counteract environmental fluctuations. The circuit achieves this because light and clock signals synergize with each other only at the early phase of the light-dark cycles. This property of the circuit adds to the remarkably diverse ways that the clock may be used by organisms. Furthermore, it might be a fitness advantage for plants to stabilize one group of molecular activities with the clock, while making other activities sensitive to the light conditions using the clock as a reference.

Physiological functions of external coincidence

Although the sensitivity of eS6-P to light around dawn has not been investigated comprehensively, experimental data showed that eS6-P rises quickly in response to light [18,22], as anticipated by our model. The general dynamical feature of eS6-P as a result of clock-light signal integration is consistent with other

known signaling events in which the coincidence of internal, clock-derived signals and external light signals drives prominent peaks of molecular activities in plants [8,9,35]. For example, according to the classic 'external coincidence' mechanism for photoperiodic (seasonal) flowering, the clock drives up the expression of the regulator of flowering, CONSTANS, late in the day. In long-day plants, if CO happens to be exposed to light late in the day, CO is activated and triggers flowering, whereas if CO is met by darkness, as is the case in the winter, flowering remains suppressed [9]. Thus, the external coincidence model allows plants to detect variation in photoperiod at the end of the day. Our work suggests another implementation of external coincidence, where variation in light conditions is detected at the beginning of the day by sensing photoperiod sensitive shifts in the phase of circadian genes[26,28]. For CO at the end of the day, coincidence of clock and light signals activates CO while darkness is incoherent with the clock, and represses CO. For comparison, according to our model eS6-P is most sensitive to changes in light conditions at the beginning of the light period because the negative effect of the clock and the potentially positive effect of light are incoherent. We propose that eS6-P helps the plant to sense variation in the onset of light, as a result of cloud cover or shading by other objects in the morning, and adjust its physiology accordingly.

Versatile performance objectives of feedforward loops

Previous studies have demonstrated multiple functions of feedforward loops in terms of systems dynamics, including accelerating responses, fold-change detection, adaptation to constant signals and filtering noise [36-39]. In addition, it was shown that a feedforward loop can perform a 'counting' function that transforms oscillatory input to stable signals [40]. Our study shows a previously underappreciated function of a particular type of feedforward loop containing an intrinsic autonomous oscillator. This system not only detects the phase and period variations of the oscillatory inputs by combining the signals

from the external and internal oscillations, but also memorizes the altered response in the following cycles, which may serve to anticipate additional perturbations. The latter feature may be useful for plants to predict weather through encoding the information in the light conditions of the previous day. This result further demonstrates the versatility of the functions of the feedforward loop. Future work is needed to determine whether this phase-detection mechanism can be integrated with other known functions of feedforward loops.

Anticipation of changes in environmental conditions

Phosphorylation of eS6 occurs in all organisms where it has been examined, including yeast, plants, and humans [12-14]. A previous study showed dramatically increased translation activity in mammalian cells with a phosphorylation-deficient eS6, suggesting a possible role of eS6-P in controlling general resource allocation in cells [15]. If this potential function of eS6-P were conserved across kingdoms, then our work would further suggest that eS6-P might tune some aspect of protein synthesis in response to variable light condition. This function, while still to be demonstrated in plants, would not be far-fetched given that translation requires a substantial input in cellular energy, which may be depleted at the end of night. This detection and anticipation of daylength may help plants to prepare for days with particular patterns of light exposures. It has been shown that growing yeast cells can allocate resources to anticipate favorable or unfavorable environmental conditions, and the choice of these anticipations may be made with rhythmic dynamics [41,42]. Regardless of the specific cellular functions of eS6-P, our work sheds light on the rich dynamics of eS6-P under fluctuating environmental conditions. Moreover, the remarkable information processing characteristic of the signaling circuit that controls eS6-P has the capacity to detect and memorize critical cues to allow plants to adapt to a dynamical light environment.

Methods

Framework of mathematical models

We modeled gene regulatory networks that control eS6-P using ordinary differential equations (ODEs). The network topologies are shown in Fig. 1. Because most interactions involving high-order molecular interactions, including transcriptional regulation and multisite phosphorylation, we used a generic form of nonlinear ODEs suitable for describing both gene expression and molecular interaction networks [43-46]. Each ODE system in the model has the form:

$$\frac{dX_i}{dt} = \gamma_i(F(\sigma_i W_i) - X_i)$$

$$F(\sigma W) = \frac{1}{(1 + e^{-\sigma W})}$$

$$W_i = (\omega_i^o + \sum_j^N \omega_{j\to i} X_j)$$

$$i = 1, \ldots, N \qquad (1)$$

Here, X_i is the activity of protein i. On a time scale $1/\gamma_i$, $X_i(t)$ relaxes toward a value determined by the sigmoidal function, F, which has a steepness set by σ. The basal value of F, in the absence of any influencing factors, is determined by ω_i^0. The coefficients $\omega_{j\to i}$ determine the influence of protein j on protein i. N is the total number of proteins in the network. Activity values are scaled from 0 (absent) to 1 (saturation). For eS6-P, we modeled a single site phosphorylation (S237) that was assumed to be independent of other phosphorylation sites, so we used first order reaction rate law that describes the phosphorylation and dephosphorylation. All variables and parameters are dimensionless. One time unit in the simulations corresponds to approximately 2.53 hours (9.5 unit per cycle), but we transformed the time unit to 1 hour for all subsequent analyses and visualizations.

The clock component of our model describes four species (LHY/CCA1, EC, PRR9/7, and PRR5/1), and the light-sensing pathway has two species (TOR and S6K). Together with eS6-P, our full Clock+Light model has seven ODEs in total. Numerical solutions to the ODEs were obtained with Tellurium [47]. Computer code for simulating the models under various conditions and reproducing key figures is available at: https://github.com/panchyni/eS6_Models.

Parameter estimation

Because the clock component of the model is independent of other elements except for the light input, we first fit the clock components of the model (4 ODEs) by applying qualitative criteria to ensure that it properly replicated features of the circadian clock [18]. We approached optimization the same way as in Locke at al. [5] and De Caluwe et al. [48] by using objective functions which impose costs on deviating from expected, qualitative behavior. Specifically, we penalized the model for (1) having the LHY/CCA1 component peak more than 1 hour before or after dawn in long (16L:8D) days, (2) having the same deviation described in (1) in 12L:12D days, (3) having a period under constant light outside of 24 to 25 hours, (4) having a period under constant darkness outside of 24 to 28 hours, and (5) having an amplitude of less than 0.1 (i.e. 10% of maximum activity) in any component. These criteria defined by intervals of desired output were used to construct an objective function to evaluate the models. When calculating the objective score, each of the five terms is zero if the output falls in the interval and is the squared difference between the output and the boundary of the interval if the output falls outside the interval. Before optimizing the model parameters, we defined a hyperbox in the parameter space that is bounded by biologically plausible parameter ranges, particularly with regard to the direction of regulation and balance of rates. A population of 40 vectors, each containing 24 parameters, generated by Latin hypercube sampling (LHS), were used as the initial estimation. Starting with this population, we implemented

576 Differential Evolution (DE) optimization algorithm [49,50] with a mutation rate between 0.35 and 0.65 and
577 a crossover rate of between 0.75 and 0.95, and let the optimization run for 15000 generations of DE or
578 the convergence of the evolution. Similar to the approach used by De Caluwe et al. [48], we then compared
579 each component to expression data from Diurnal Database [27] which were normalized onto a 0 to 1 scale
580 to ensure the estimated component activity approximated the proper phase and shape of actual clock
581 components (Fig. S2) We performed 250 runs of such optimization to ensure that the performance of the
582 selected parameter set can be reproduced. For fitting eS6-P, we selected among viable models which
583 accurately reflected clock behavior and selected the one with the greatest dynamic range of among the
584 clock components.
585
586 Next, we used the time course measurement of eS6-P to estimate the parameters controlling the
587 regulation of eS6-P by clock components (LHY/CCA1, EC, PRR97, and PRR51 which correspond to C1, C2,
588 C3, and C4 respectively) and the light induced TOR pathway [18]. The data set has Western Blot
589 quantification of eS6-P for 78 hours at a 6-hour interval. In the model, the eS6-P variable describes the
590 percentage of the amount of eS6-P with respect to the total eS6. We therefore inferred the fractions of
591 eS6-P from the Western Blot quantification of the experiment and scaled these values based on an
592 approximation of the eS6-P saturation value inferred from Williams et al. [51]. 2D-gel electrophoresis data
593 from this study suggest that a majority, but not all eS6 undergoes phosphorylation and that
594 phosphorylation spreads across several sites which may or may not be phosphorylated at the same time
595 (see Fig. 4 and Table 1 in [51]). As the data were not quantified in the original study and estimations based
596 on image analysis were broad (15-77% per site), we chose a conservative estimate of 0.40 as the saturating
597 value. This normalization gives the raw data a range of 0.01 to 0.4 and pooled data (described below) a
598 range of average values from 0.06 to 0.31. This procedure allows us to avoid unrealistic assumptions with
599 either no phosphorylated (eS6-P = 0) or fully phosphorylated (eS6-P = 1) in the system. Because these

values are approximate and mainly meant to avoid fitting to unrealistic, extreme values of eS6-P, the model describes eS6-P in arbitrary units (a. u.) rather than actual percentages.

We regularized the transformed data by pooling the data points from the same Zeitgeber time, and we used the pooled mean and variance for each time point to calculate the log likelihood. Constant light was emulated in the model by fixing the value of light to 1 and the CCA1 overexpression by fixing the basal production of CCA1 to 50. To examine steady state behavior under each condition, we entrained the model with one day of darkness followed by ten days of the given condition, before comparing the model to the experimental data on the twelfth day. The objective function for the parameter optimization was defined by the log-likelihood function that quantifies the fit of the simulation results to the experimental data with variabilities. Log likelihood estimates for all time points of eS6-P contribute to the objective function equally in an additive manner. As with clock components, we used the DE based optimization algorithm to estimate the remaining parameters. All algorithmic parameters were the same as the optimization for the clock component, expect for the maximum number of generations (5000). We performed 1400 optimization runs, and among the optimized parameter sets we selected the best preforming model with a moderate peak to perform subsequent analyses. Note that the majority of the models in the lowest 5th percentile of likelihood values exhibited the same behavior as the chosen model, including cycling under all three experimental conditions and an early eS6-P peak under LD conditions (Fig. S3A). Models with larger likelihood scores (the next 5 percentiles) show neither this earlier peak nor cycling under constant light (Fig. S3B). A full list of model parameters can be found in Table S1.

Applying a detailed clock to our eS6-P model

In addition to our simplified 4-component clock model, we also tested our eS6-P model using a more detailed circadian clock component from De Caluwe et al. [48], which has the same overall network

623 topology but explicitly considers protein and mRNA concentrations (Fig. S4). We added our equation for
624 eS6-P regulation to this full clock model, and used the set of same optimized parameters that we obtained
625 from the simplified model to simulate eS6-P with the light-dark cycle. The CCA1 constitutive
626 overexpression mutant was simulated by removing the clock and light regulated components from the
627 equations for CCA1/LHY transcription (i.e. setting the production rate to maximum). We used the protein
628 concentration of each pair of clock components, representing the mean protein concentration of the two
629 gene products, in place of our generalized clock component activity values. We scaled the concentration
630 values to a range of [0,1] using the minimum and maximum values of that protein pair. However, in the
631 case of CCA1 overexpression, we assumed that the concentration is effectively saturated at the maximum
632 wild-type value, as the average value of CCA1/LHY and PRR9/7 increased by more than five-fold. All
633 parameters for eS6 regulation were the same as in the model in Fig. 1, except for the regulatory effect of
634 the TOR pathway which was increased by 10% to avoid an unrealistic saturation point of eS6-P under wild-
635 type and CCA1 overexpression conditions.

636

637 **Alternative models**

638 To illustrate the unique performance of the Clock+Light model that contains the clock component, we
639 built three alternative models that describe plausible ways in which the eS6-P can transmit the light signal
640 to achieve detection of daylength variations at the beginning of a day. Note that it is trivial for a system
641 to detect daylength variations at the end of a day (e.g. through integration of, or slow response to, light
642 signals), and this detection may not be as useful as the early day detection in terms of anticipating
643 environmental changes. The three alternative models are: 1) a linear circuit that transmits light signals to
644 eS6-P (Fig. 3A, top panel), 2) an incoherent feedforward loop (IFFL) that produces an early day peak similar
645 to what the Clock+Light model does under LD condition (Fig. 3A and B, middle panels), and 3) a coherent

feedforward loop (CFFL) that allows slow decline of eS6-P upon the withdrawal of light signals (Fig. 3A, lower panel). Parameter values of these models were manually chosen to give characteristic responses (Fig. 3A, Table S2).

Mutual information between daylength variations and eS6-P responses

To examine the transmitted information from daylength variations (signal) to eS6-P abundance (response) when the system is subject to external or internal noise, we introduced uncorrelated multiplicative white noise to ODEs for the light and eS6-P as $dx/dt = f(x_1, x_2, \ldots, x_n) + \mu_x \cdot x \cdot dW$, where dW is a Wiener process that can be discretized as $dW \sim N(0,1) \cdot \sqrt{dt}$ where $N(0,1)$ denotes a normally distributed random variable with zero mean and unit variance, and μ_x represents the amplitude of the fluctuation. To quantify the information transmission, we used mutual information between signal S and response R [52]. In the eS6-P system, S represents the perturbation of the time (Δt_{ND}) at which the system receives light signal from a normal light-dark cycle (e.g. 12hr light and 12hr dark), and R represents the eS6-P abundance. The responses were the maximum eS6-P levels in the 4-hour time window after dawn. The calculation of the mutual information was performed with the discretized form [53]:

$$I(S;R) = -\sum_{i}^{S_B} \frac{k_{s,i}}{N_T} \log \frac{k_{s,i}}{N_T} + \sum_{j}^{R_B} \frac{k_{r,j}}{N_T} \sum_{i}^{S_B} \frac{k_{i,j}}{N_T} \log \frac{k_{i,j}}{N_T} \quad (2)$$

Here, signals values were assigned to S_B bins, and the response values were assigned to R_B bins. By binning all signals and responses, we constructed a contingency matrix of which each entry is the number of observations from the simulated data that correspond to that particular signal-response pair. N_T is the sum over all entries in the table, and $k_{i,j}$ is the number of instances of signal i that resulted in response j. In this study, 21 signal bins and 10 response bins were used. Using more response or signal bins will likely increase the mutual information, so our analysis focuses on comparisons of lower bounds of the mutual

668 information. The bounds of the response bins were determined by the minimal and maximal responses in
669 the absence of the noise. For each signal value, 200 simulations were performed.

670

671 **Photoperiod data processing**

672 We obtained a copy of the NOAA Solar Calculator (https://www.esrl.noaa.gov/gmd/grad/solcalc/
673 calcdetails.html) and generated approximated day length information (i.e. Sunlight Duration) for a full
674 year for three locations: Oslo, Norway (59.91 Latitude, 110.75 Longitude), Praia, Cape Verde (14.92
675 Latitude, -23.51 Longitude), and Boston, Massachusetts (42.35 Latitude, -71.05 Longitude). For inclusion
676 in our model, we fit a model of day-night variation to each data set with the following form:

677 $$L = a + b \cdot \sin\left(\frac{2\pi d}{365} - c\pi\right) + \sin\left(\frac{2\pi t}{T}\right) \quad (3)$$

678 where the rightmost sine term represents a base 12-hr light/dark cycles and the leftmost sine term
679 modulates this average day based on the time of the year. Here, d is the day of the year, t is the time of
680 day in hours and T is the period of the day in hours. The parameters a, b, and c, are fit such that the
681 fraction of daylight ($L > 0$) conforms to the NOAA estimations for each day (values for each location are
682 listed in Table S6). With this idealized year-long data, the time for analysis of daily response is based the
683 natural light condition rather than any artificially defined time. We also obtained measurement of
684 radiation data in the Harvard Forest [30] including downward oriented photosynthetically active radiation
685 (par.down), which we used as an approximation for daylight. A threshold value (9.0) was used to define
686 day/night using par.down and was chosen such that it minimized the average difference between the
687 inferred hours of daylight and NOAA estimations of day length across all days binned by month. For
688 inclusion in our model, we smoothed radiation data from 2006 (which had the fewest missing values)
689 using cubic splines and applied the threshold to generate binary day/night values.

690

691 **Identification of genes with time-series expression profiles similar to eS6-P dynamics**

692 To identify genes that show similar cyclic patterns to eS6-P dynamics under LD, LL and CCA1
693 overexpression conditions, we first selected genes identified by Dalchau et al. [8] where the peak
694 expression in long-day was during the early day (ZT 0-6 hours) but the peak expression in constant light
695 was during subjective night (ZT 18-24 hours). There were 126 genes that satisfy these conditions. We then
696 used the RNA sequencing data from Missra et al. (measurement under CCA1 overexpression condition) to
697 further filter these genes. We selected genes that had both peak expression during the day, and a
698 difference between average expression during the day and night of at least 25% of the peak value under
699 CCA1 overexpression condition. To visualize the time course profiles of these genes, we used data from
700 Diurnal Database for LD [27], Edwards et al. for LL [32], and Missra et al. for CCA1 overexpression [10].

701 For gene ontology (GO) analysis, we used all 92 eS6-P like genes and tested for enrichment against all *A.*
702 *thaliana* genes using PANTHER ([54]; available through http://geneontology.org/). The same procedure
703 we used when testing all genes identified by Dalchau et al.[8]. *p*-values were calculated using the Fisher's
704 exact test and multiple test correction was done using Benjamini-Hochberg method with a false discovery
705 rate threshold of 0.05.

706 Dalchau et al. classified the genes with cyclic expression patterns into three categories: light-dominant,
707 clock dominant and co-regulated [8]. To examine which category the eS6-P profile would belong to, we
708 used the same approach to classifying light/clock regulation as Dalchau et al. by comparing the ratio of
709 eS6-P amplitude driven by the clock (constant light) to that driven by the light-dark cycle. Briefly,
710 amplitude difference between LL condition and LD condition was used to determine whether light or clock
711 dominates the regulation of each gene. With our eS6-P data, the amplitude under the LD condition is
712 higher than that under LL condition by 2.17 fold (difference in Bode magnitude = -3.3 decibels, dB), which

713 categorizes eS6 phosphorylation as a process co-regulated by light and clock according to the cutoffs

714 (±7dB difference in Bode magnitude), although light regulation is favored.

715 **References**

716 1. Dodd AN, Salathia N, Hall A, Kévei E, Tóth R, et al. (2005) Plant circadian clocks increase
717 photosynthesis, growth, survival, and competitive advantage. Science 309. 5734: 630-633.

718 2. Turek FW, Joshu C, Kohsaka A, Lin E, Ivanova G, et al. (2005) Obesity and metabolic syndrome in
719 circadian Clock mutant mice. Science 308. 5724: 1043-1045.

720 3. Shim JS, Kubota A, Imaizumi T (2017) Circadian clock and photoperiodic flowering in Arabidopsis:
721 CONSTANS is a hub for signal integration. Plant Physiol 173. 1: 5-15.

722 4. Pokhilko A, Fernández AP, Edwards KD, Southern MM, Halliday KJ, et al. (2012) The clock gene circuit
723 in Arabidopsis includes a repressilator with additional feedback loops. Mol Syst Biol 8. 1.

724 5. Locke JCW, Kozma-Bognár L, Gould PD, Fehér B, Kevei E, et al. (2006) Experimental validation of a
725 predicted feedback loop in the multi-oscillator clock of Arabidopsis thaliana. Mol Syst Biol 2. 1.

726 6. Harmer SL, Hogenesch JB, Straume M, Chang H-S, Han B, et al. (2000) Orchestrated transcription of
727 key pathways in Arabidopsis by the circadian clock. Science 290. 5499: 2110-2113.

728 7. Michael TP, Mockler TC, Breton G, McEntee C, Byer A, et al. (2008) Network discovery pipeline
729 elucidates conserved time-of-day–specific cis-regulatory modules. PLoS Genet 4. 2.

730 8. Dalchau N, Hubbard KE, Robertson FC, Hotta CT, Briggs HM, et al. (2010) Correct biological timing in
731 Arabidopsis requires multiple light-signaling pathways. Proc Natl Acad Sci U S A 107. 29: 13171-
732 13176.

733 9. Salazar JD, Saithong T, Brown PE, Foreman J, Locke JCW, et al. (2009) Prediction of photoperiodic
734 regulators from quantitative gene circuit models. Cell 139. 6: 1170-1179.

735 10. Missra A, Ernest B, Lohoff T, Jia Q, Satterlee J, et al. (2015) The circadian clock modulates global daily
736 cycles of mRNA ribosome loading. The Plant Cell 27. 9: 2582-2599.

737 11. Xu X, Hotta CT, Dodd AN, Love J, Sharrock R, et al. (2007) Distinct light and clock modulation of
738 cytosolic free Ca2+ oscillations and rhythmic CHLOROPHYLL A/B BINDING PROTEIN2 promoter
739 activity in Arabidopsis. The Plant Cell 19. 11: 3474-3490.

740 12. Chauvin C, Koka V, Nouschi A, Mieulet V, Hoareau-Aveilla C, et al. (2014) Ribosomal protein S6 kinase
741 activity controls the ribosome biogenesis transcriptional program. Oncogene 33. 4: 474.

742 13. Meyuhas O (2015) Ribosomal protein S6 phosphorylation: four decades of research. Int Rev Cell Mol
743 Biol: Elsevier. pp. 41-73.

744 14. Yerlikaya S, Meusburger M, Kumari R, Huber A, Anrather D, et al. (2016) TORC1 and TORC2 work
745 together to regulate ribosomal protein S6 phosphorylation in Saccharomyces cerevisiae. Mol Biol Cell
746 27. 2: 397-409.

747 15. Ruvinsky I, Katz M, Dreazen A, Gielchinsky Y, Saada A, et al. (2009) Mice deficient in ribosomal
748 protein S6 phosphorylation suffer from muscle weakness that reflects a growth defect and energy
749 deficit. PLoS One 4. 5: e5618.

750 16. Biever A, Valjent E, Puighermanal E (2015) Ribosomal protein S6 phosphorylation in the nervous
751 system: from regulation to function. Front Mol Neurosci 8: 75.

752 17. Dobrenel T, Mancera-Martinez E, Forzani C, Azzopardi M, Davanture M, et al. (2016) The Arabidopsis
753 TOR kinase specifically regulates the expression of nuclear genes coding for plastidic ribosomal
754 proteins and the phosphorylation of the cytosolic ribosomal protein S6. Frontiers in plant science 7:
755 1611.

756 18. Enganti R, Cho SK, Toperzer JD, Urquidi-Camacho RA, Cakir OS, et al. (2018) Phosphorylation of
757 ribosomal protein RPS6 integrates light signals and circadian clock signals. Frontiers in plant science
758 8: 2210.

759 19. Choudhary MK, Nomura Y, Wang L, Nakagami H, Somers DE (2015) Quantitative circadian
760 phosphoproteomic analysis of Arabidopsis reveals extensive clock control of key components in
761 physiological, metabolic, and signaling pathways. Mol Cell Proteomics 14. 8: 2243-2260.

762 20. Magnuson B, Ekim B, Fingar DC (2012) Regulation and function of ribosomal protein S6 kinase (S6K)
763 within mTOR signalling networks. Biochem J 441. 1: 1-21.

764 21. Schmelzle T, Hall MN (2000) TOR, a central controller of cell growth. Cell 103. 2: 253-262.

765 22. Chen G-H, Liu M-J, Xiong Y, Sheen J, Wu S-H (2018) TOR and RPS6 transmit light signals to enhance
766 protein translation in deetiolating Arabidopsis seedlings. Proc Natl Acad Sci U S A 115. 50: 12823.

767 23. Pfeiffer A, Janocha D, Dong Y, Medzihradszky A, Schöne S, et al. (2016) Integration of light and
768 metabolic signals for stem cell activation at the shoot apical meristem. Elife 5: e17023.

769 24. Bujdoso N, Davis SJ (2013) Mathematical modeling of an oscillating gene circuit to unravel the
770 circadian clock network of Arabidopsis thaliana. Frontiers in Plant Science 4: 3.

771 25. Avello PA, Davis SJ, Ronald J, Pitchford JW (2019) Heat the Clock: Entrainment and Compensation in
772 Arabidopsis Circadian Rhythms. Journal of circadian rhythms 17.

773 26. Fogelmark K, Troein C (2014) Rethinking transcriptional activation in the Arabidopsis circadian clock.
774 PLoS Comput Biol 10. 7.

775 27. Mockler TC, Michael TP, Priest HD, Shen R, Sullivan CM, et al. (2007) The DIURNAL project: DIURNAL
776 and circadian expression profiling, model-based pattern matching, and promoter analysis. Cold
777 Spring Harb Symp Quant Biol 72: 353-363.

778 28. Webb AAR, Seki M, Satake A, Caldana C (2019) Continuous dynamic adjustment of the plant
779 circadian oscillator. Nature communications 10. 1: 1-9.

780 29. Weigel D (2012) Natural variation in Arabidopsis: from molecular genetics to ecological genomics.
781 Plant Physiol 158. 1: 2-22.

782 30. Moore KE, Fitzjarrald DR, Sakai RK, Goulden ML, Munger JW, et al. (1996) Seasonal variation in
783 radiative and turbulent exchange at a deciduous forest in central Massachusetts. Journal of Applied
784 Meteorology 35. 1: 122-134.

785 31. Yanovsky MJ, Kay SA (2002) Molecular basis of seasonal time measurement in Arabidopsis. Nature
786 419. 6904: 308.

787 32. Edwards KD, Anderson PE, Hall A, Salathia NS, Locke JCW, et al. (2006) FLOWERING LOCUS C
788 mediates natural variation in the high-temperature response of the Arabidopsis circadian clock. The
789 Plant Cell 18. 3: 639-650.

790 33. Troein C, Locke JCW, Turner MS, Millar AJ (2009) Weather and seasons together demand complex
791 biological clocks. Curr Biol 19. 22: 1961-1964.

792 34. Gonze D, Halloy J, Goldbeter A (2002) Robustness of circadian rhythms with respect to molecular
793 noise. Proc Natl Acad Sci U S A 99. 2: 673-678.

794 35. Seaton DD, Graf A, Baerenfaller K, Stitt M, Millar AJ, et al. (2018) Photoperiodic control of the
795 Arabidopsis proteome reveals a translational coincidence mechanism. Mol Syst Biol 14. 3.

796 36. Mangan S, Itzkovitz S, Zaslaver A, Alon U (2006) The incoherent feed-forward loop accelerates the
797 response-time of the gal system of Escherichia coli. J Mol Biol 356. 5: 1073-1081.

798 37. Ghosh B, Karmakar R, Bose I (2005) Noise characteristics of feed forward loops. Phys Biol 2. 1: 36.

799 38. Mangan S, Alon U (2003) Structure and function of the feed-forward loop network motif. Proc Natl
800 Acad Sci U S A 100. 21: 11980-11985.

801 39. Goentoro L, Shoval O, Kirschner MW, Alon U (2009) The incoherent feedforward loop can provide
802 fold-change detection in gene regulation. Mol Cell 36. 5: 894-899.

803 40. Zhang C, Tsoi R, Wu F, You L (2016) Processing oscillatory signals by incoherent feedforward loops.
804 PLoS Comput Biol 12. 9: e1005101.

805 41. Gurvich Y, Leshkowitz D, Barkai N (2017) Dual role of starvation signaling in promoting growth and
806 recovery. PLoS Biol 15. 12: e2002039.

807 42. Metzl-Raz E, Kafri M, Yaakov G, Soifer I, Gurvich Y, et al. (2017) Principles of cellular resource
808 allocation revealed by condition-dependent proteome profiling. Elife 6.

809 43. Watanabe K, Panchy N, Noguchi S, Suzuki H, Hong T (2019) Combinatorial perturbation analysis
810 reveals divergent regulations of mesenchymal genes during epithelial-to-mesenchymal transition. npj
811 Syst Biol Appl 5. 1: 21.

812 44. Hong T, Xing J, Li L, Tyson JJ (2012) A simple theoretical framework for understanding heterogeneous
813 differentiation of CD4+ T cells. BMC Syst Biol 6. 1: 66-66.

814 45. Hong T, Xing J, Li L, Tyson JJ (2011) A Mathematical Model for the Reciprocal Differentiation of T
815 Helper 17 Cells and Induced Regulatory T Cells. PLoS Comput Biol 7. 7: e1002122-e1002122.

816 46. Mjolsness E, Sharp DH, Reinitz J (1991) A connectionist model of development. J Theor Biol 152. 4:
817 429-453.

818 47. Choi K, Medley JK, König M, Stocking K, Smith L, et al. (2018) Tellurium: an extensible python-based
819 modeling environment for systems and synthetic biology. Biosystems 171: 74-79.

820 48. De Caluwé J, Xiao Q, Hermans C, Verbruggen N, Leloup J-C, et al. (2016) A compact model for the
821 complex plant circadian clock. Frontiers in plant science 7: 74.

822 49. Hong T, Oguz C, Tyson JJ (2015) A Mathematical Framework for Understanding Four-Dimensional
823 Heterogeneous Differentiation of CD4+ T Cells. Bull Math Biol 10.1007/s11538-015-0076-6: 1-19.

824 50. Ye Y, Kang X, Bailey J, Li C, Hong T (2019) An enriched network motif family regulates multistep cell
825 fate transitions with restricted reversibility. PLoS Comput Biol 15. 3: e1006855.

826 51. Williams AJ, Werner-Fraczek J, Chang IF, Bailey-Serres J (2003) Regulated phosphorylation of 40S
827 ribosomal protein S6 in root tips of maize. Plant Physiol 132. 4: 2086-2097.

828 52. Shannon CE (1948) A mathematical theory of communication. Bell system technical journal 27. 3:
829 379-423.

830 53. Cheong R, Rhee A, Wang CJ, Nemenman I, Levchenko A (2011) Information transduction capacity of
831 noisy biochemical signaling networks. Science 334. 6054: 354-358.

832 54. Mi H, Muruganujan A, Casagrande JT, Thomas PD (2013) Large-scale gene function analysis with the
833 PANTHER classification system. Nat Protoc 8. 8: 1551.

834

835

836

837 **Supporting Information**

838 **Table S1: Parameter values of the Clock+Light model**

839 **Table S2: Parameter values of alternative models**

840 **Table S3: Genes with time course expression profiles similar to dynamics of eS6-P**

841 **Table S4: GO terms enriched in eS6-P like genes**

842 **Table S5: GO terms enriched in all genes with cyclic expression patterns**

843 **Table S6: Parameter values for yearly daylength models**

844

845

846

847 **Fig. S1. The cyclic behavior of the clock model**. The behavior of the clock modules under constant long
848 days (16L:8D), transition from long-days to constant light and transition from long-days to constant dark.
849 The four components of the clock are indicated by color (red = LHY/CCA1 = C1, orange = PRR9/7 = C3,
850 green = PRR5/1 = C4, blue = EC = C2). The grey shaded area indicates the night phase of the light-dark
851 cycle.

852

853 **Fig. S2. Comparison of the clock model to the expression of circadian factors from the Diurnal Database**.
854 Simulated activity (black) is plotted against normalized expression of circadian factors that are indicated
855 by color (red = LHY and CCA1, orange = PRR9 and PPR7, green = PRR5 and PRR1, blue = ELF4 and LUX) [27].
856 Long day (16L:8D) data/simulations are on the right, and short day (8L:16D) data/simulations are on the
857 left. The grey shaded area indicates the night phase of the light-dark cycle. Experimental and model values
858 were scaled to [0, 1] based on the minima and maxima.

859

860 **Fig. S3. Performance of the eS6-P model using alternatively optimized parameters sets. (A)** Behavior of
861 the eS6-P model using the top 70 (5%) parameter sets among the 1400 optimization runs under long-day
862 (top), CCA1-overexpression (middle) and constant light (bottom) conditions. The black curve indicates the
863 experimental data to which the models were fit, and each red curve is a trajectory generated from a
864 parameter set. The grey shaded area indicates the night phase of the light-dark cycle or subjective night
865 in the case of constant light. Note that these models are consistent with the model in Fig. 1E in terms of
866 overall score and specific features, including an early day peak under a regular long-day and cyclic
867 behavior under constant light. **(B)** Behavior of the eS6-P model using the next 70 optimized parameter
868 sets under long-day (top), CCA1-overexpression (middle) and constant light (bottom) conditions. The black
869 curve indicates the experimental data to which the models were fit, and each red curve is a trajectory

generated from a parameter set. The grey shaded area indicates the night phase of the light-dark cycle or subjective night in the case of constant light.

Fig. S4. Simulations based on a model of eS6-P using a detailed circadian clock model from De Caluwe et al. [48]. Trajectories from simulations (black) are compared to observations from long-day (top), CCA1-overexpression (middle) and constant light (bottom) conditions. Circadian time is measured in hours relative to subjective dawn and shaded grey regions indicate periods of subjective night. See Methods for details of this clock model.

Fig. S5. Response of eS6-P to variation in the night to day transition time over consecutive days. (A) Diagram of perturbations of the night to day transition and the effect on length of the day relative to a normal 12L:12D day for two consecutive perturbed days. The extent of the day is shown by yellow shaded regions and the extent of the change in day length is shown by differential shading. **(B)** Early day behavior of eS6-P on the second day in response to varying the night to day transition time from $\Delta t_{ND} = -4$ (purple) to $\Delta t_{ND} = 4$ (yellow) in 1-hour increments for two consecutive days. Each model was measured for 8 hours after dawn as the shortest day is 8 hours. **(C)** The difference in eS6-P predicted by the model around the first and second dawn. The difference over the last eight hours before dusk (grey) is shown on the left and the difference in the first eight hours after dawn (white) is shown on the right. **(D)** Early day peak metric (ratio of the early day maximum of eS6-P to the eS6-P levels at the dusk) of eS6-P across different degrees of dawn variation on two consecutive days. Thin solid lines show early eS6-P response on the second day, while thicker transparent lines show early eS6-P response on the first day.

Fig. S6. Detection of daylength variations with early-day eS6-P response in the presence of light fluctuations and concentration fluctuations. **(A)** Five representative trajectories from simulations of the Clock+Light model (Fig. 1E). For each simulation, the system first reached the steady state under 12-hour light and 12-hour dark condition. Next, a perturbation of the time at which the light is turned on was performed at the dawn (Δt_{ND}, positive perturbation represents postponed dawn time). Trajectories were aligned at the actual dawn. To model fluctuations of light, a white noise term with an amplitude parameter μ=3 was added to the differential equation describing the light signal (see Methods). Red curve shows a representative light signal is shown. **(B)** Five representative trajectories from simulations with noise term on eS6-P (μ=3). **(C)** Contingency tables summarizing the relationship between daylength variations and the early eS6-P levels under the conditions in **(A)** and **(B)**. 200 stochastic simulations were performed for each daylength. eS6-P responses were categorized into 10 bins, and 21 daylength variations were tested. **(D)** Mutual information between daylength variations (represented by Δt_{ND}) and the early eS6-P levels. Multiple noise amplitudes were analyzed for the two conditions indicated.

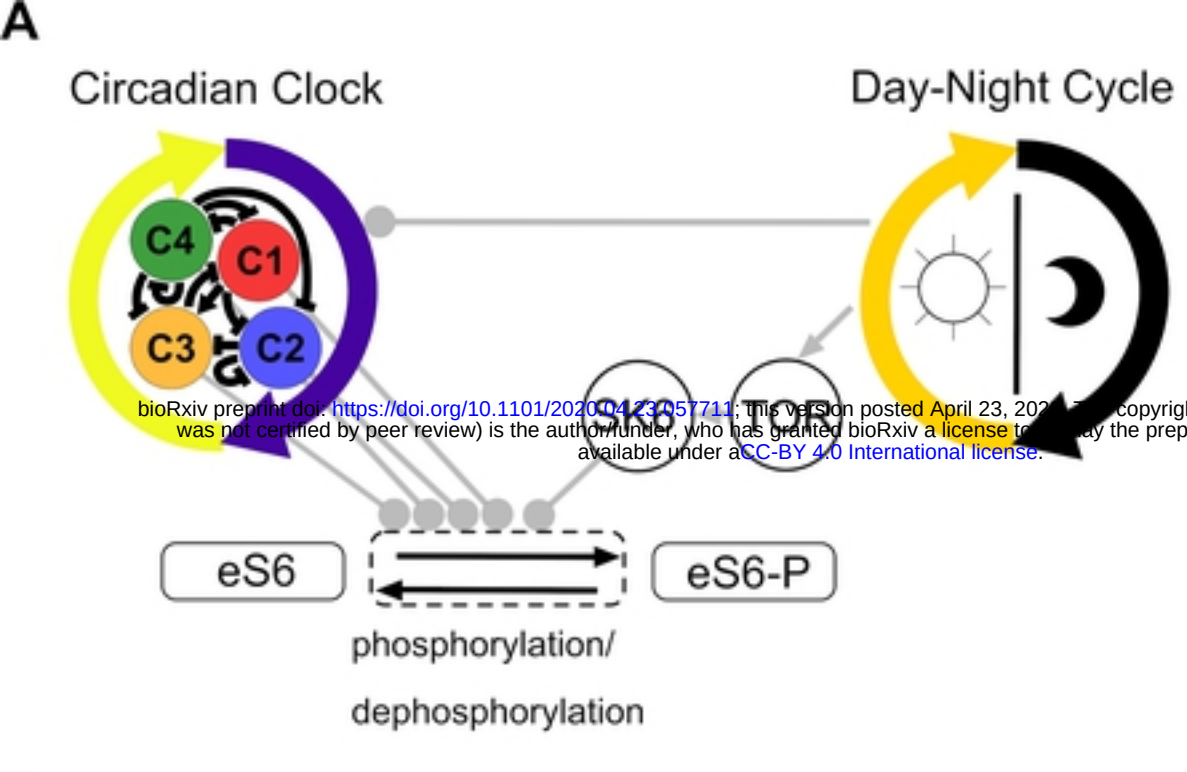

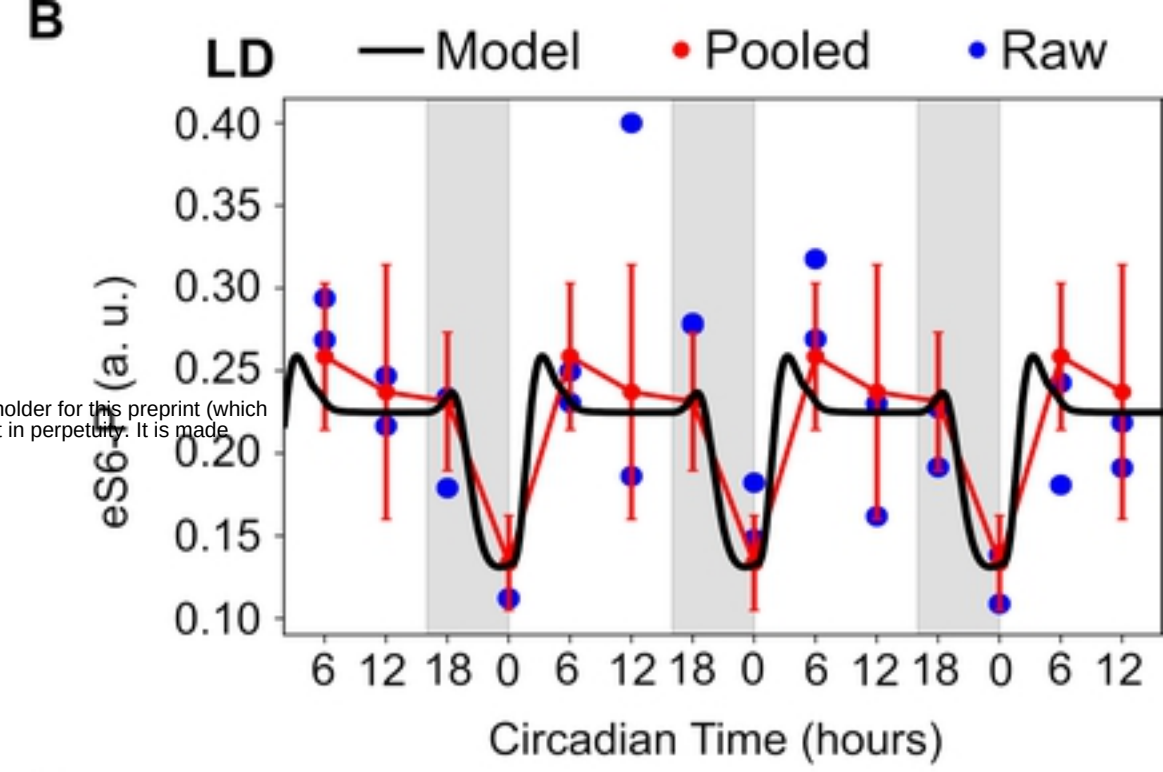

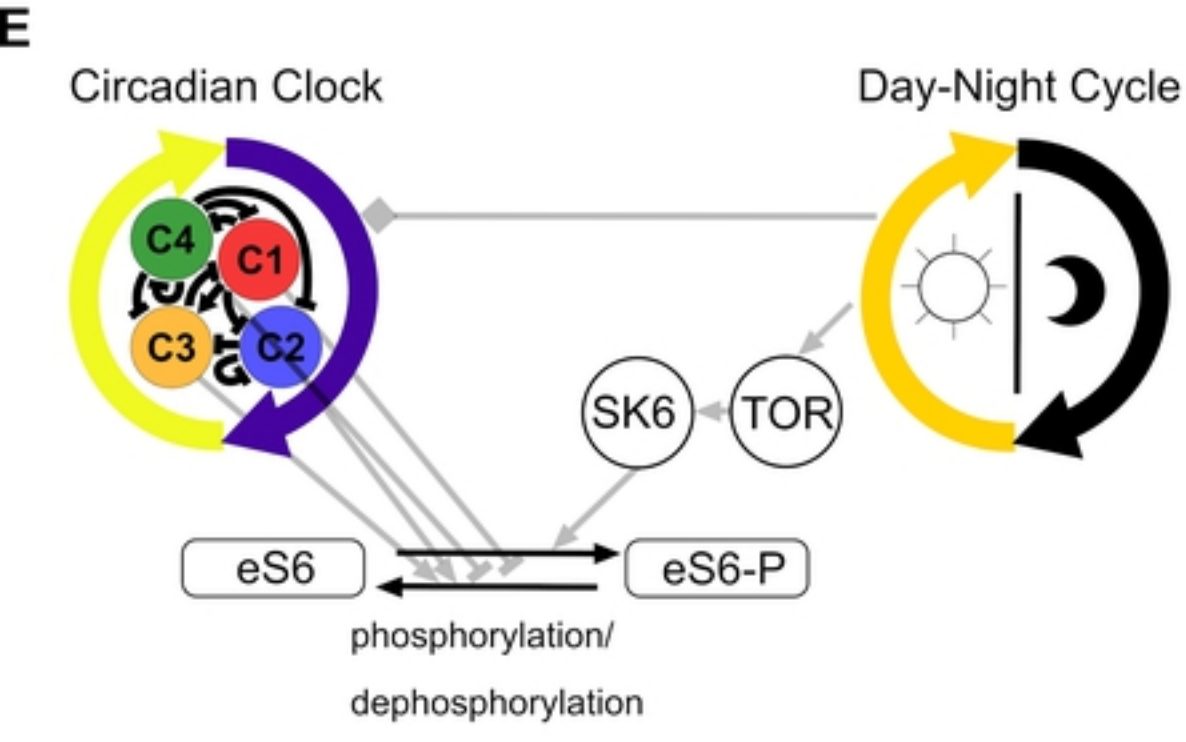

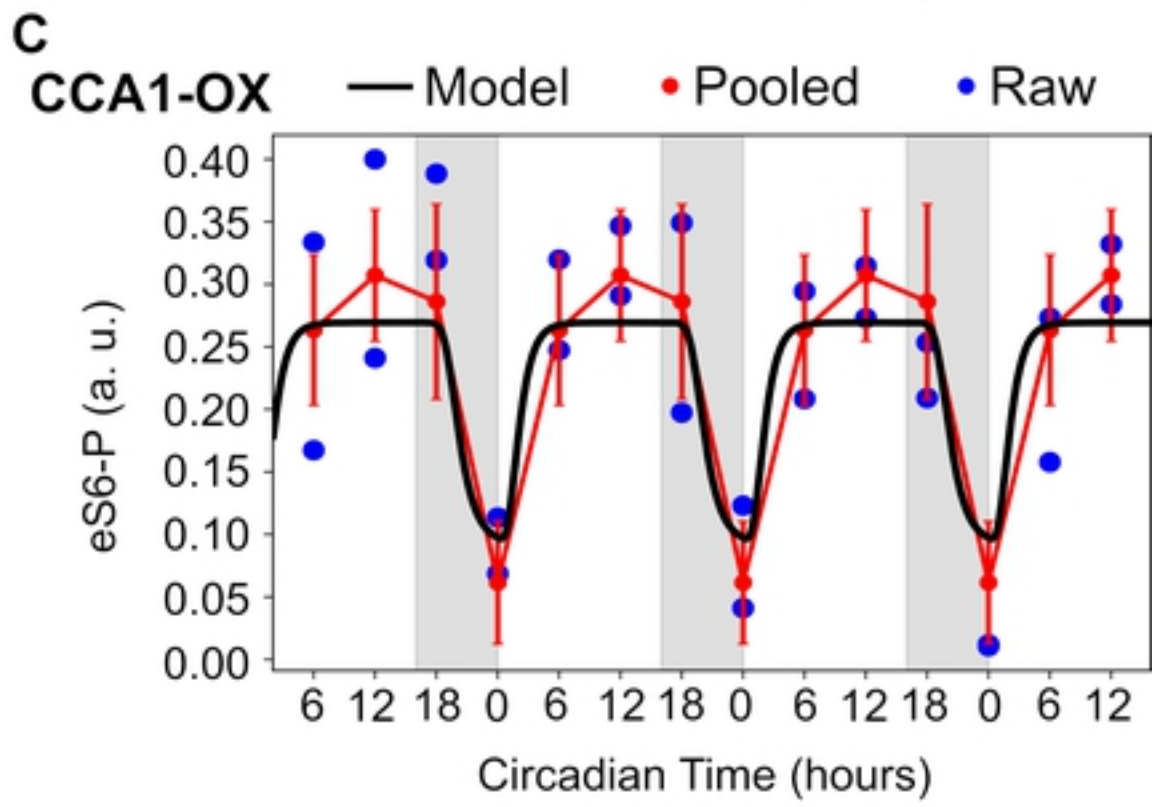

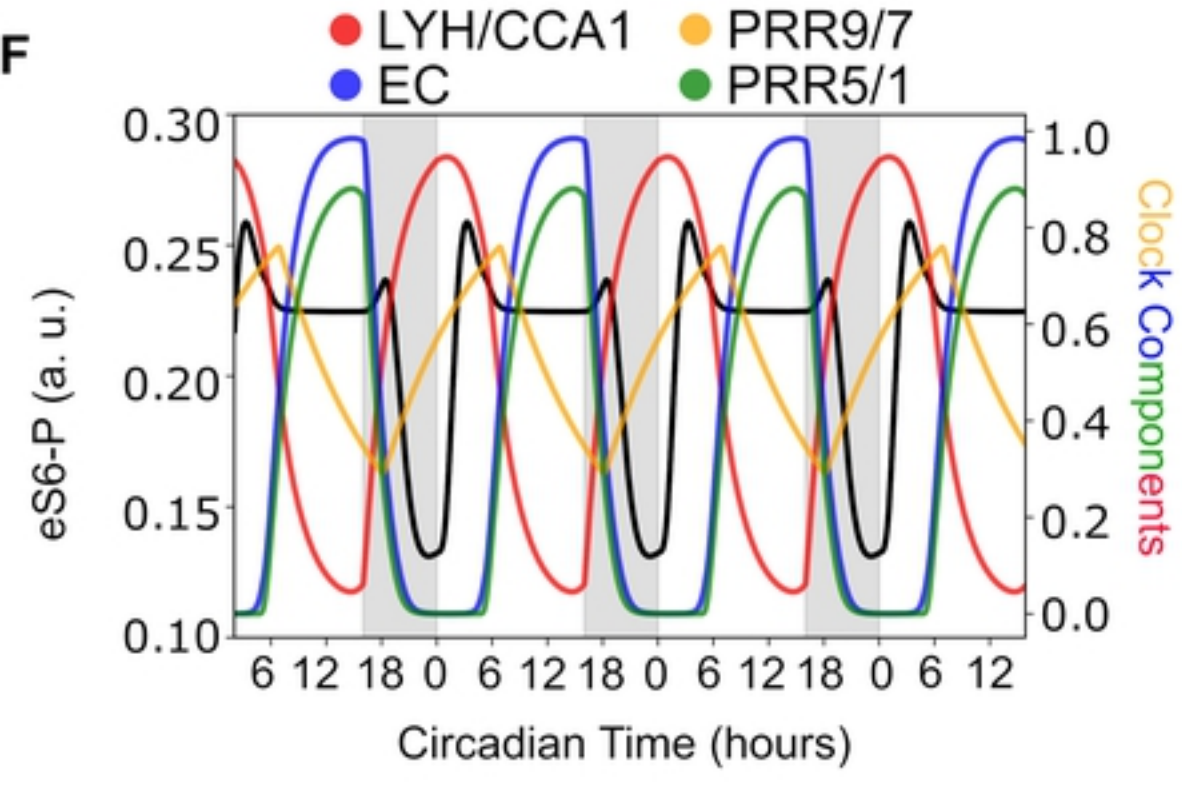

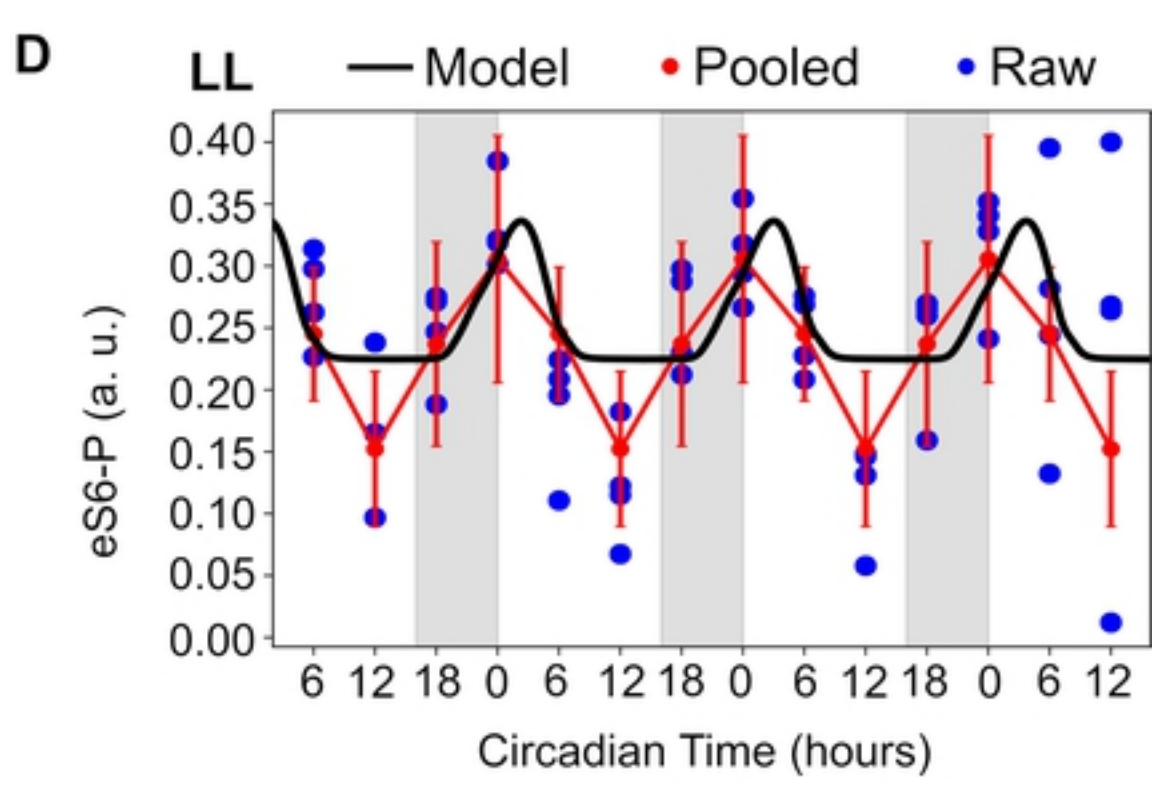

Figure 1

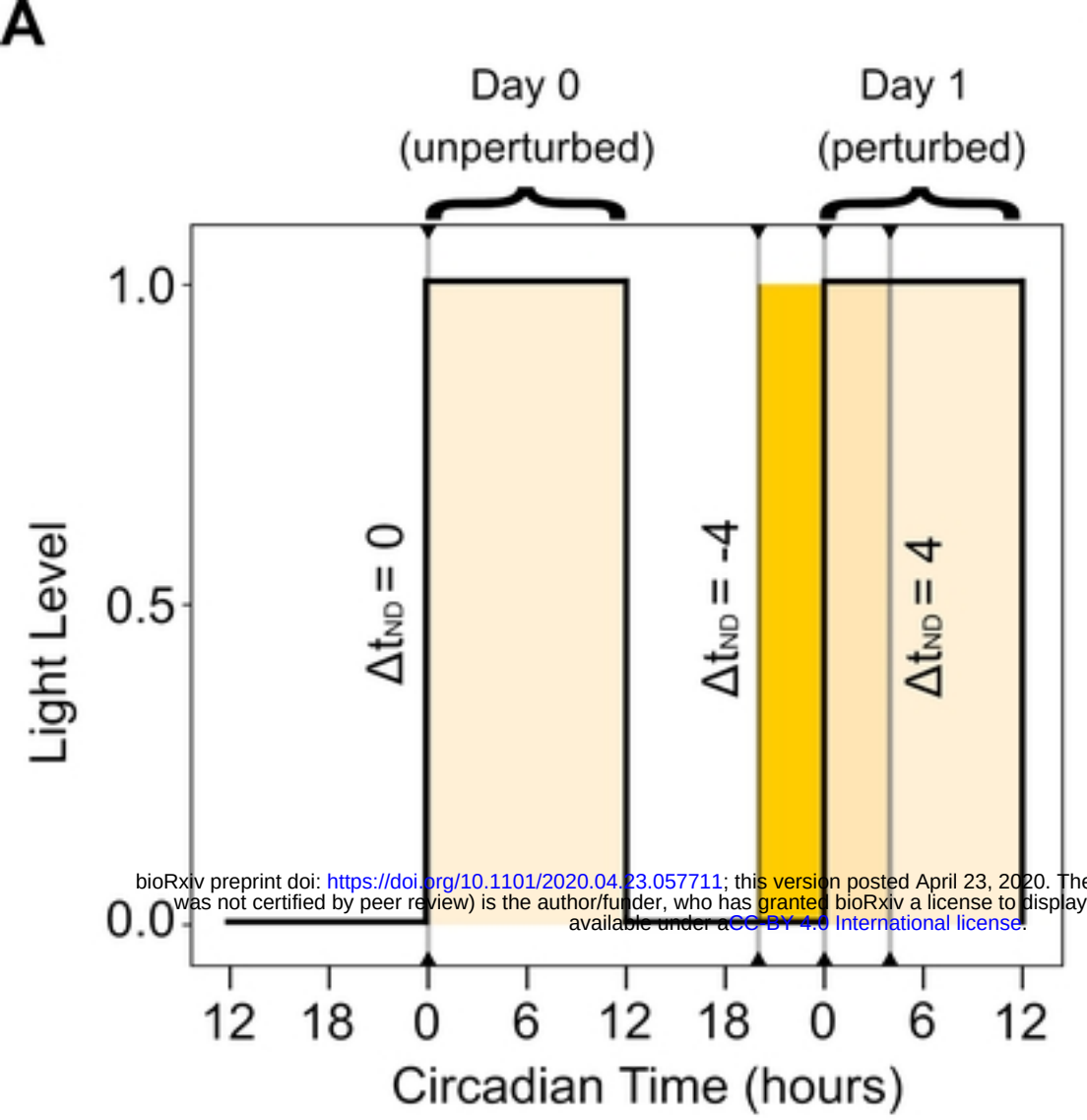

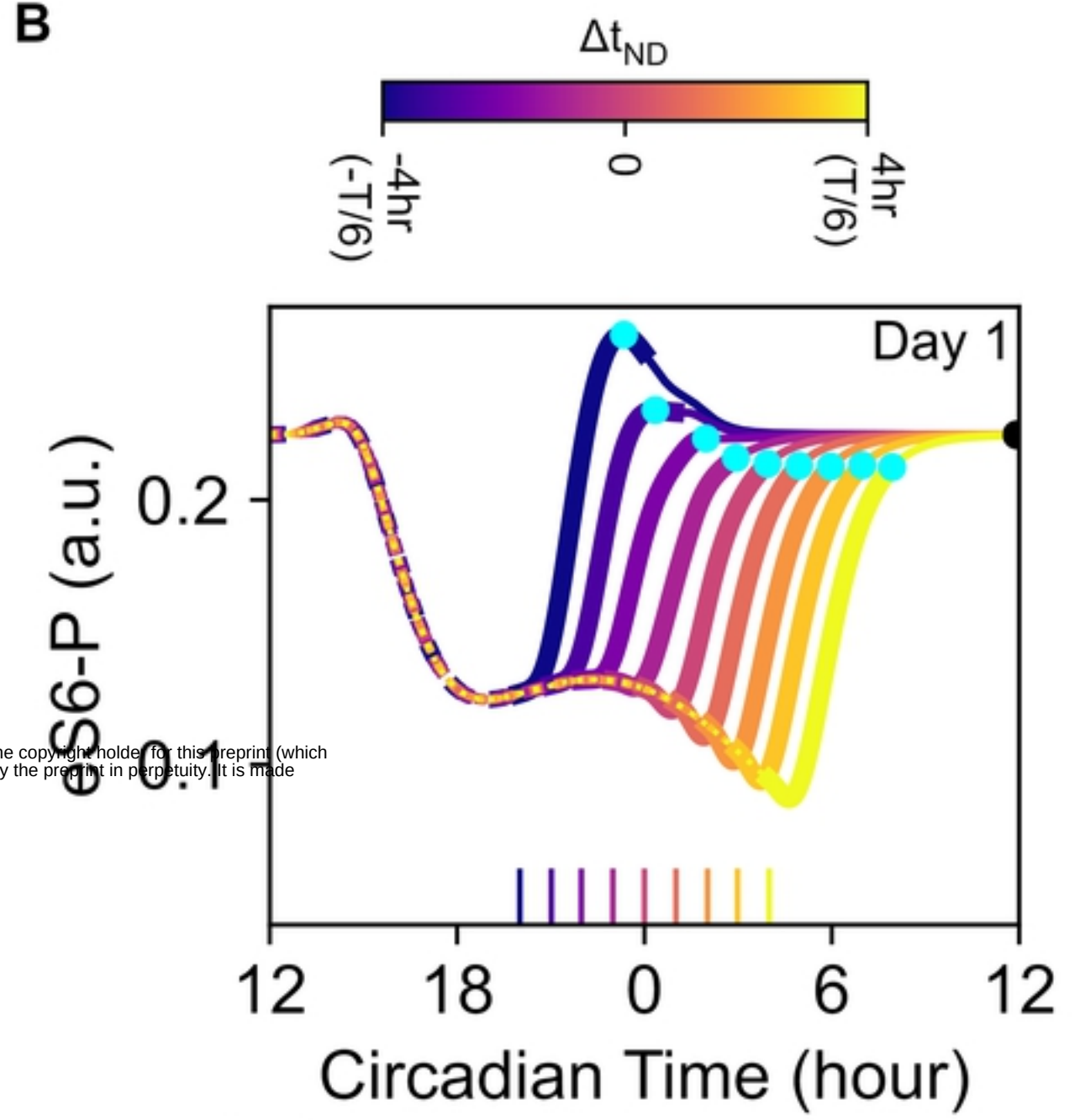

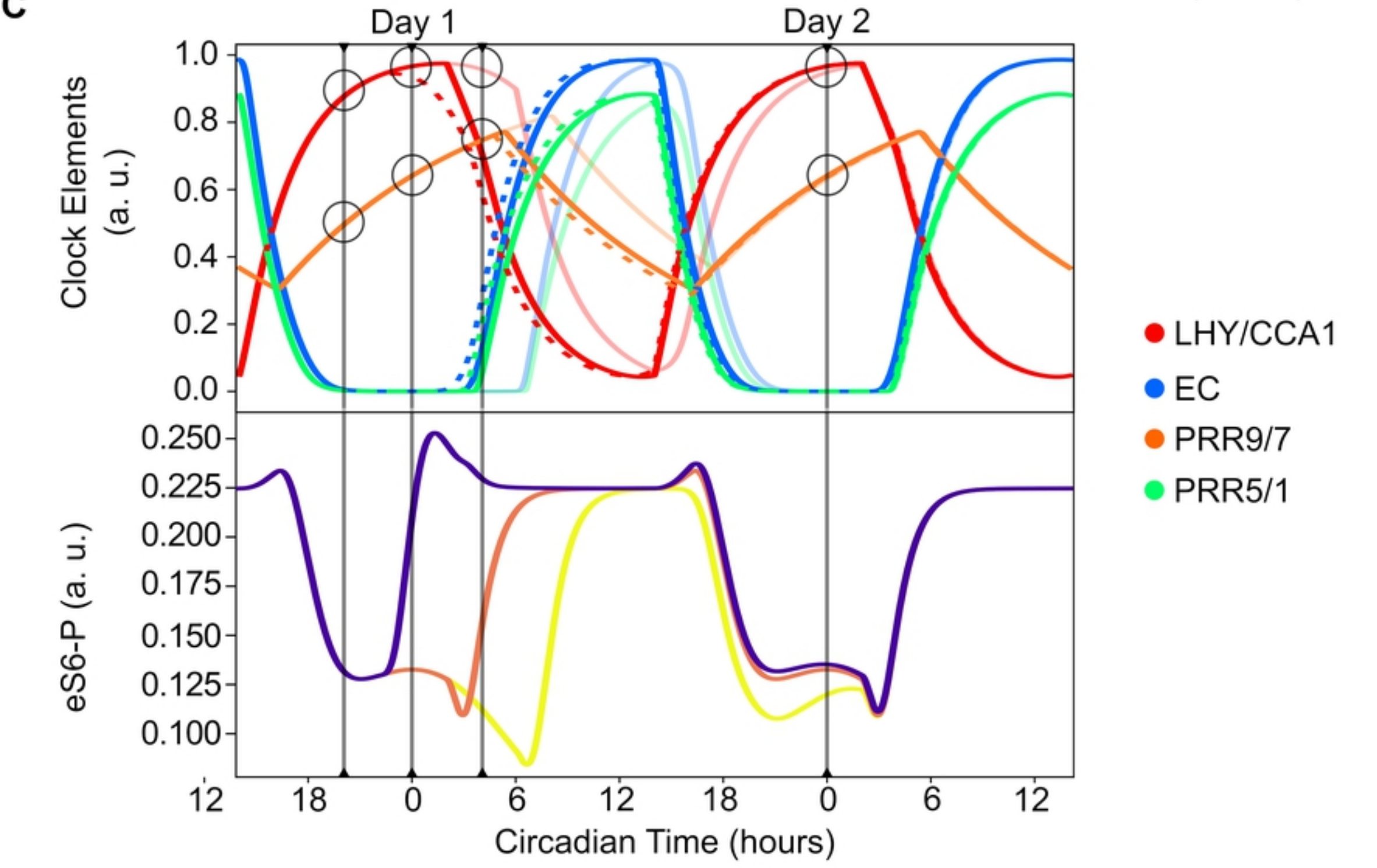

Figure 2

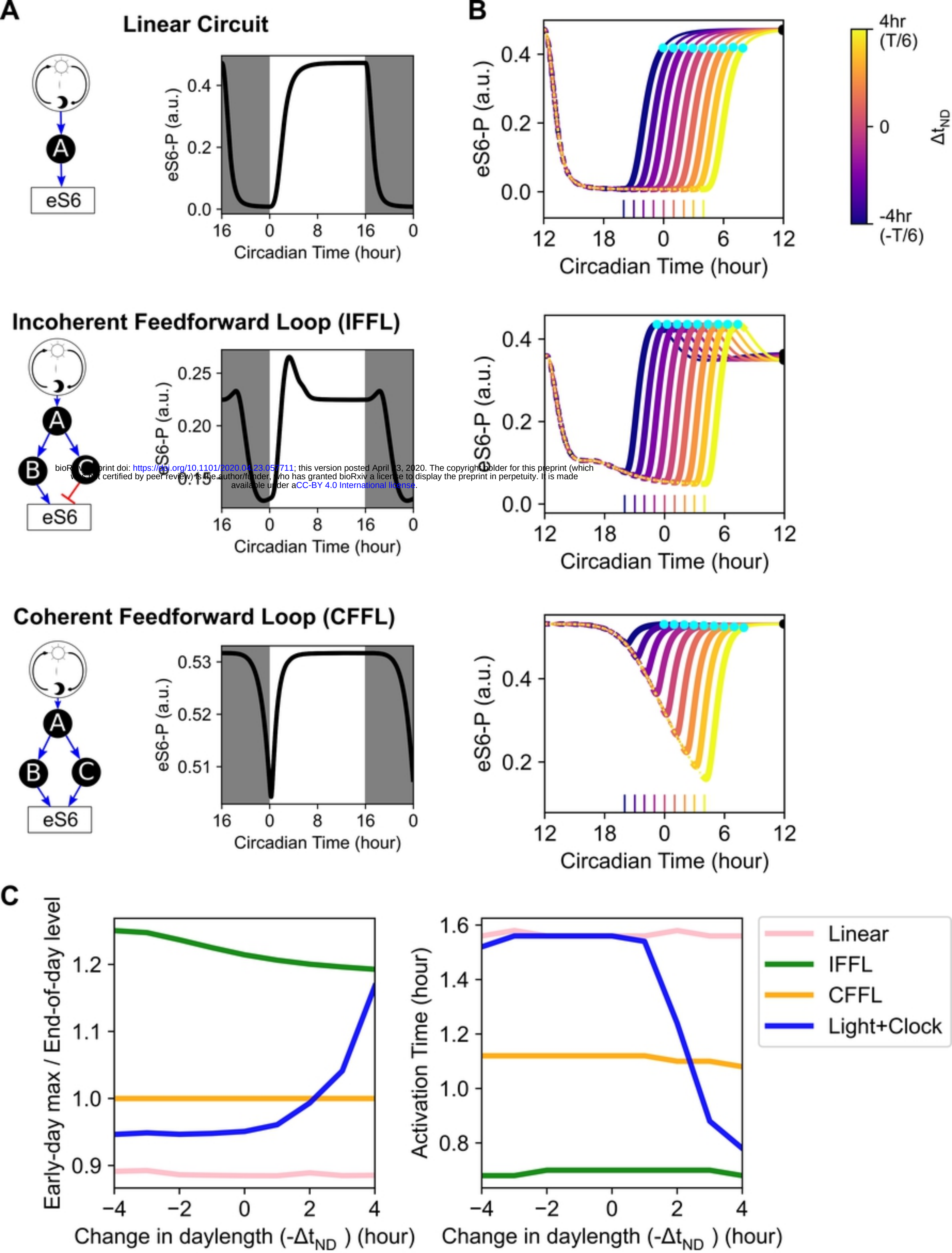

Figure 3

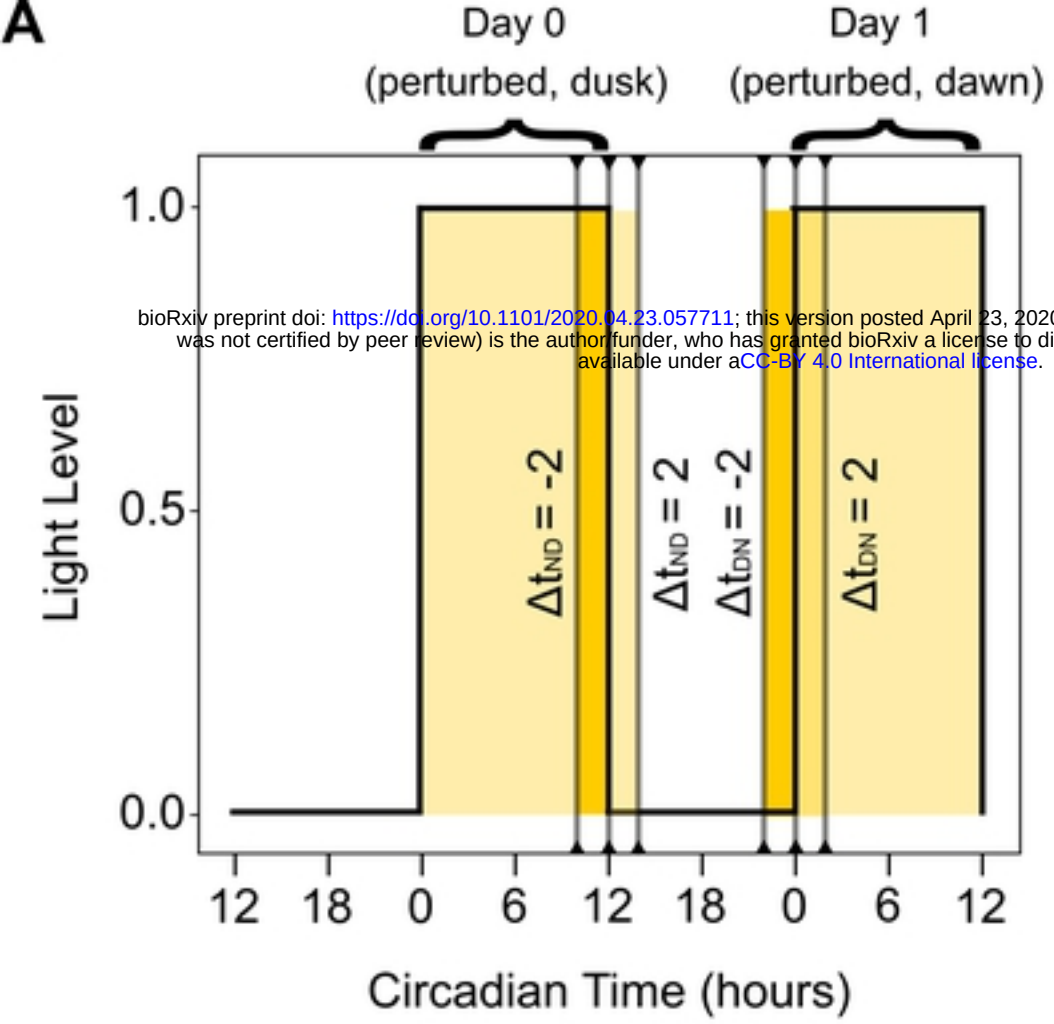

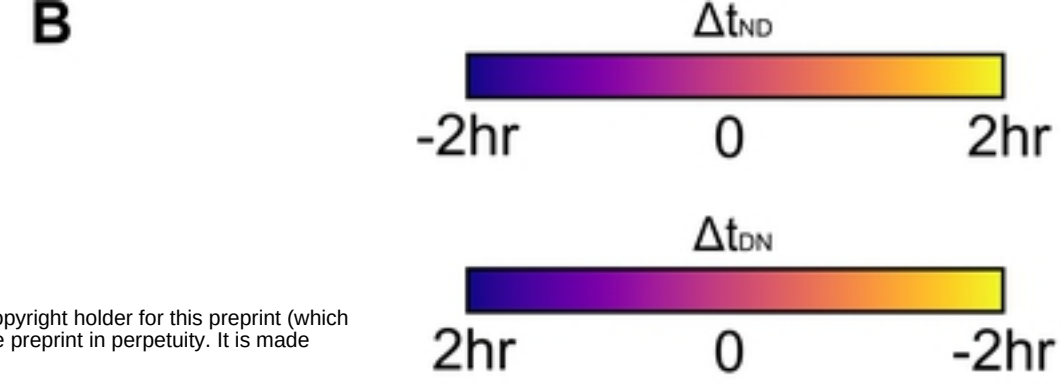

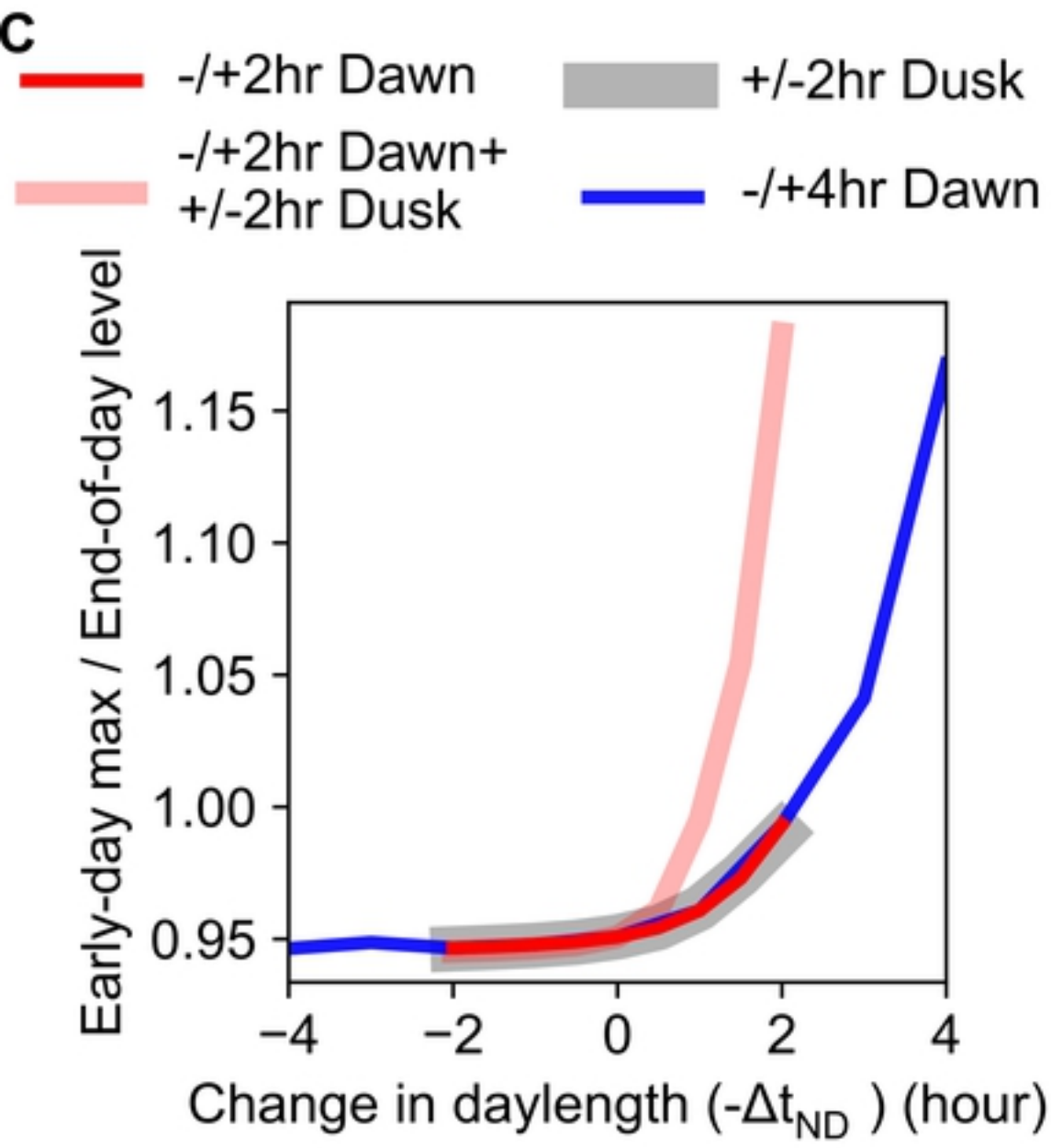

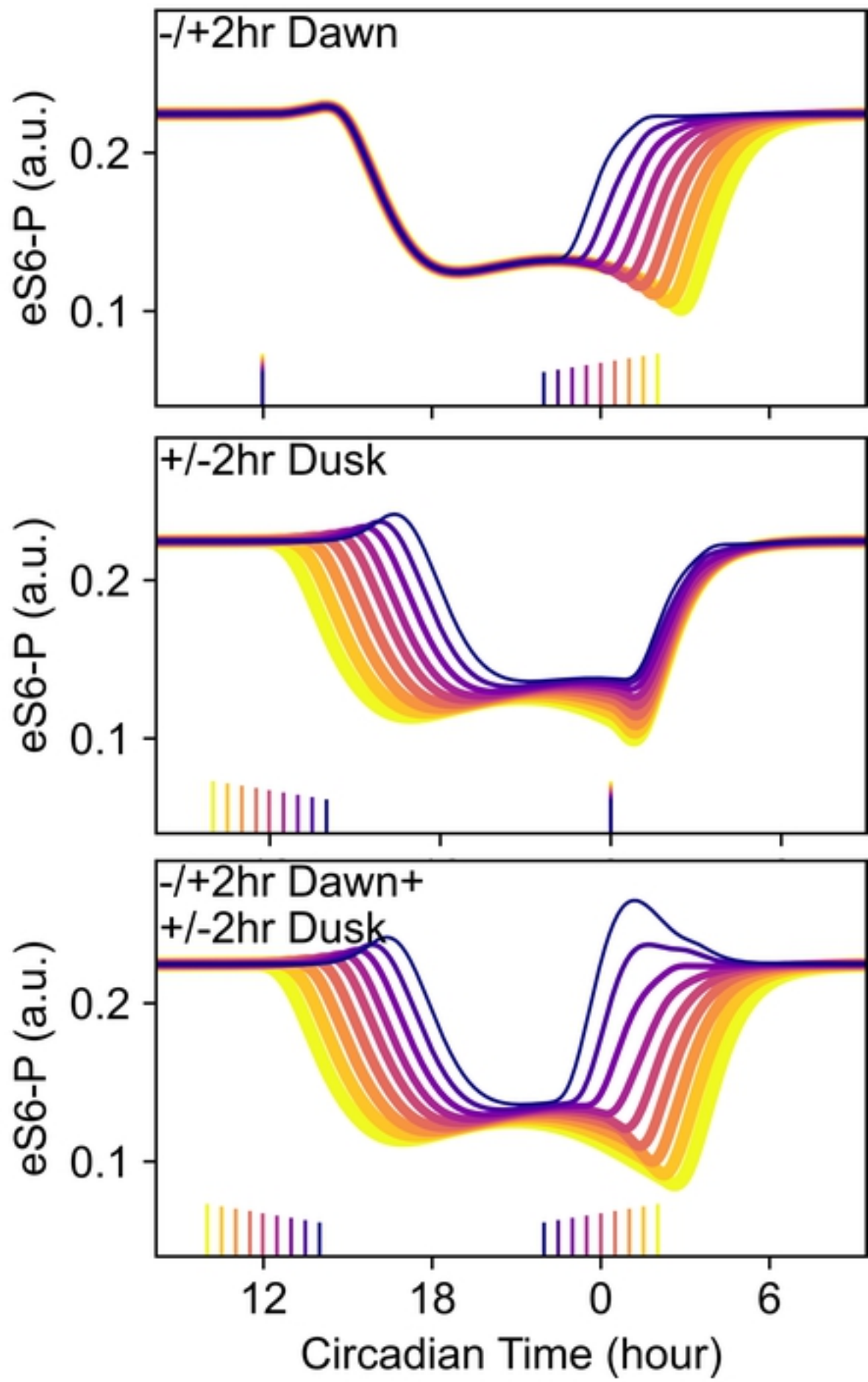

Figure 4

A

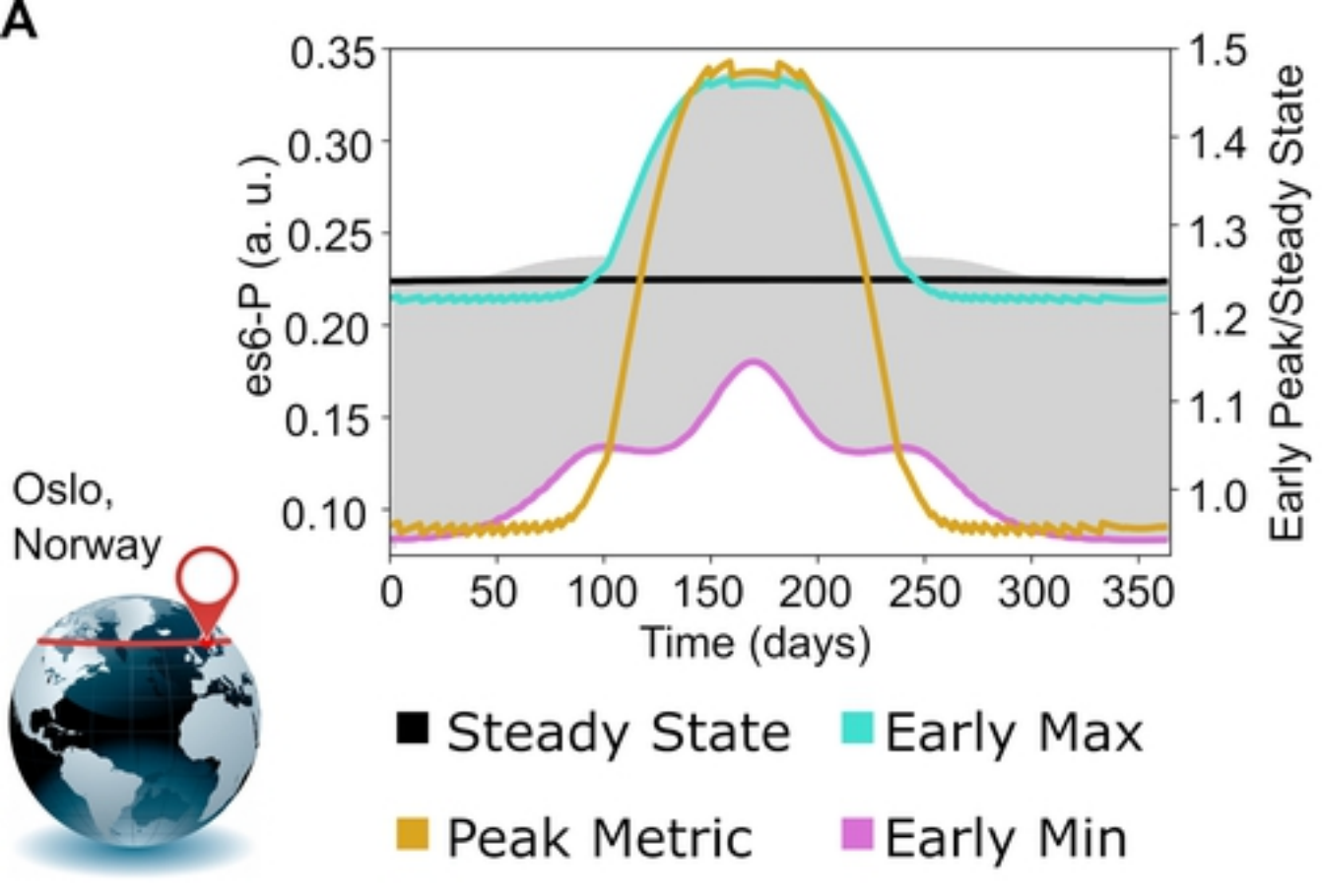
es6-P (a. u.)
Early Peak/Steady State
Time (days)
Oslo,
Norway
Steady State
Early Max
Peak Metric
Early Min

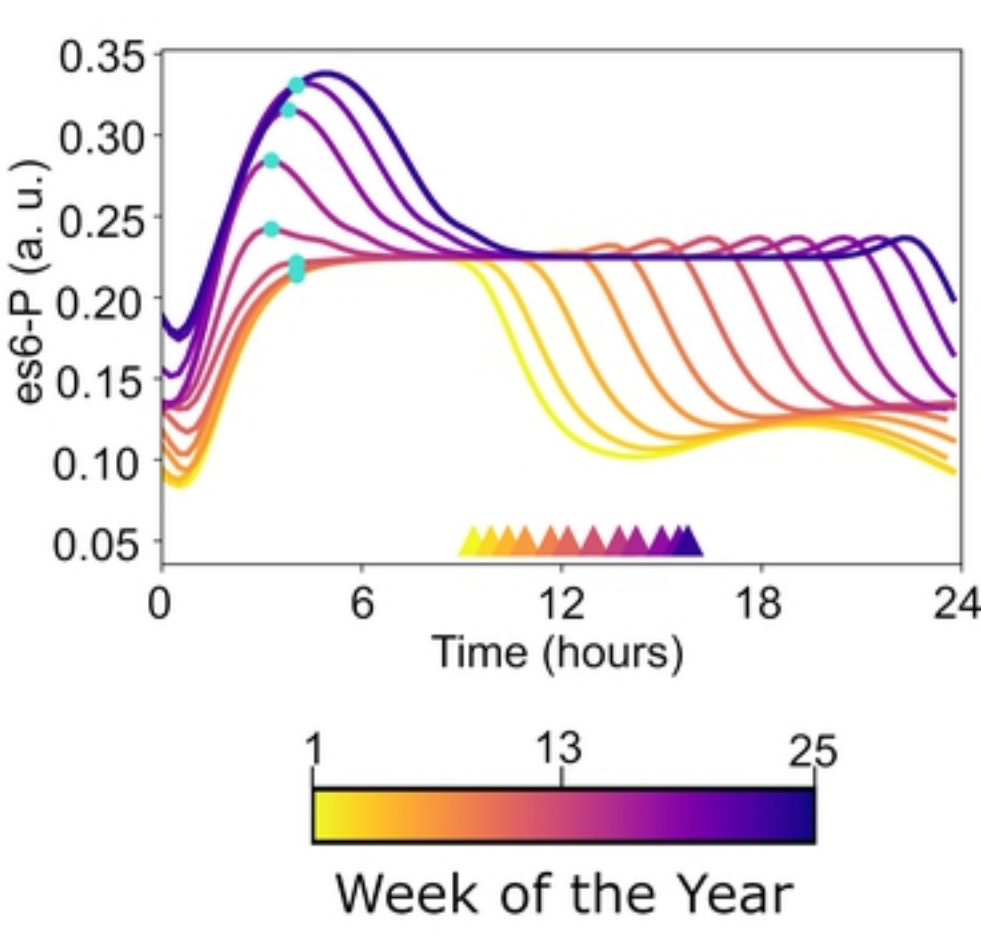
es6-P (a. u.)
Time (hours)
1
13
25
Week of the Year

B

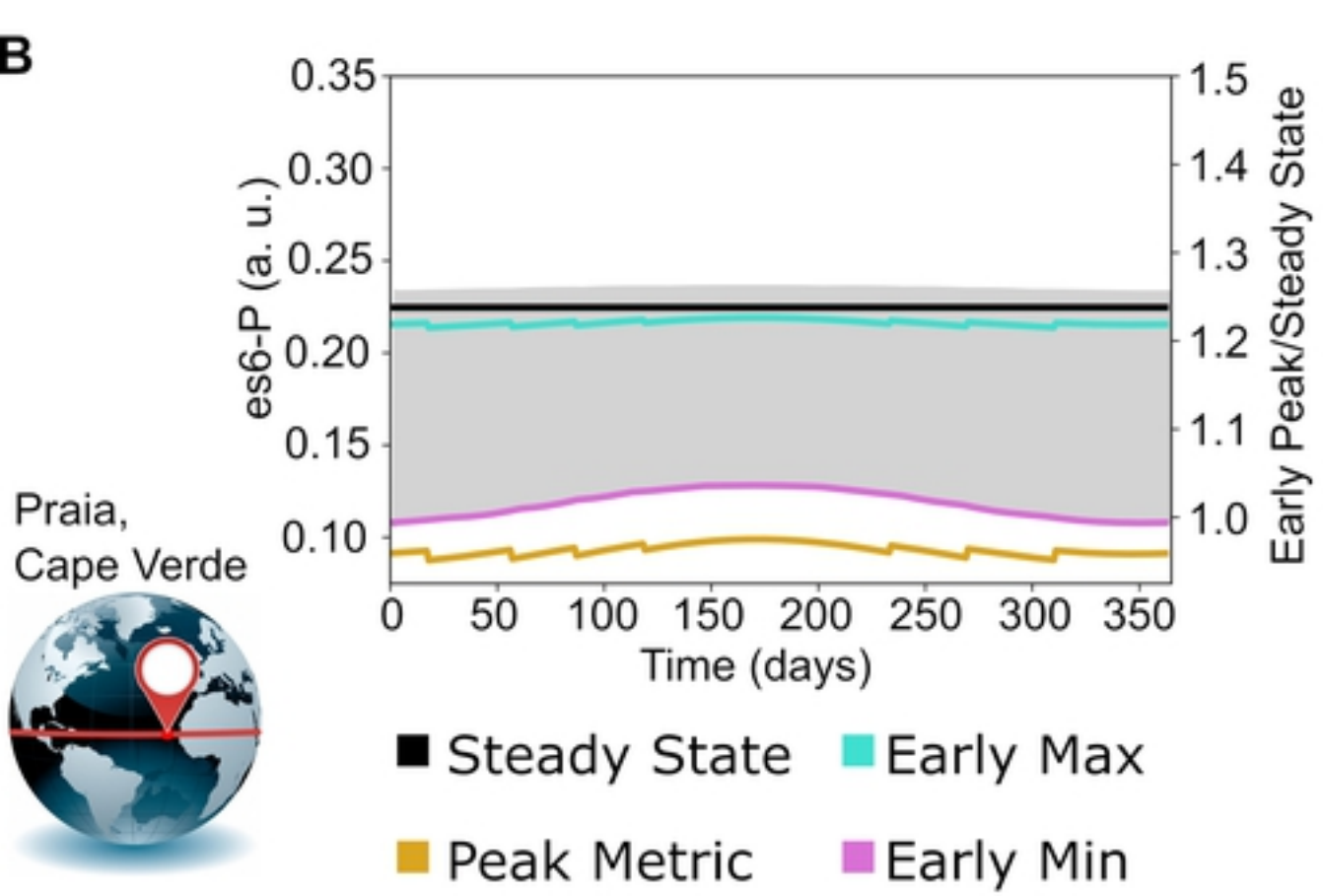
es6-P (a. u.)
Early Peak/Steady State
Time (days)
Praia,
Cape Verde
Steady State
Early Max
Peak Metric
Early Min

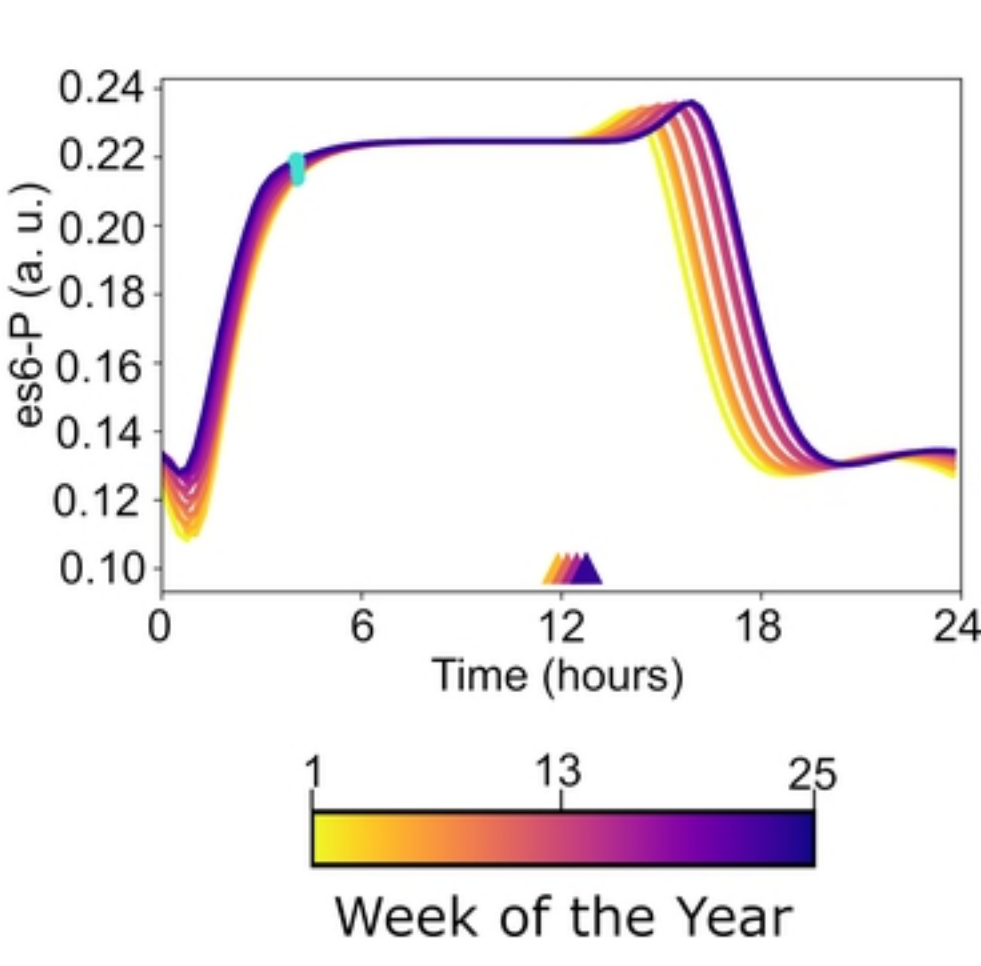
es6-P (a. u.)
Time (hours)
1
13
25
Week of the Year

Figure 5

A

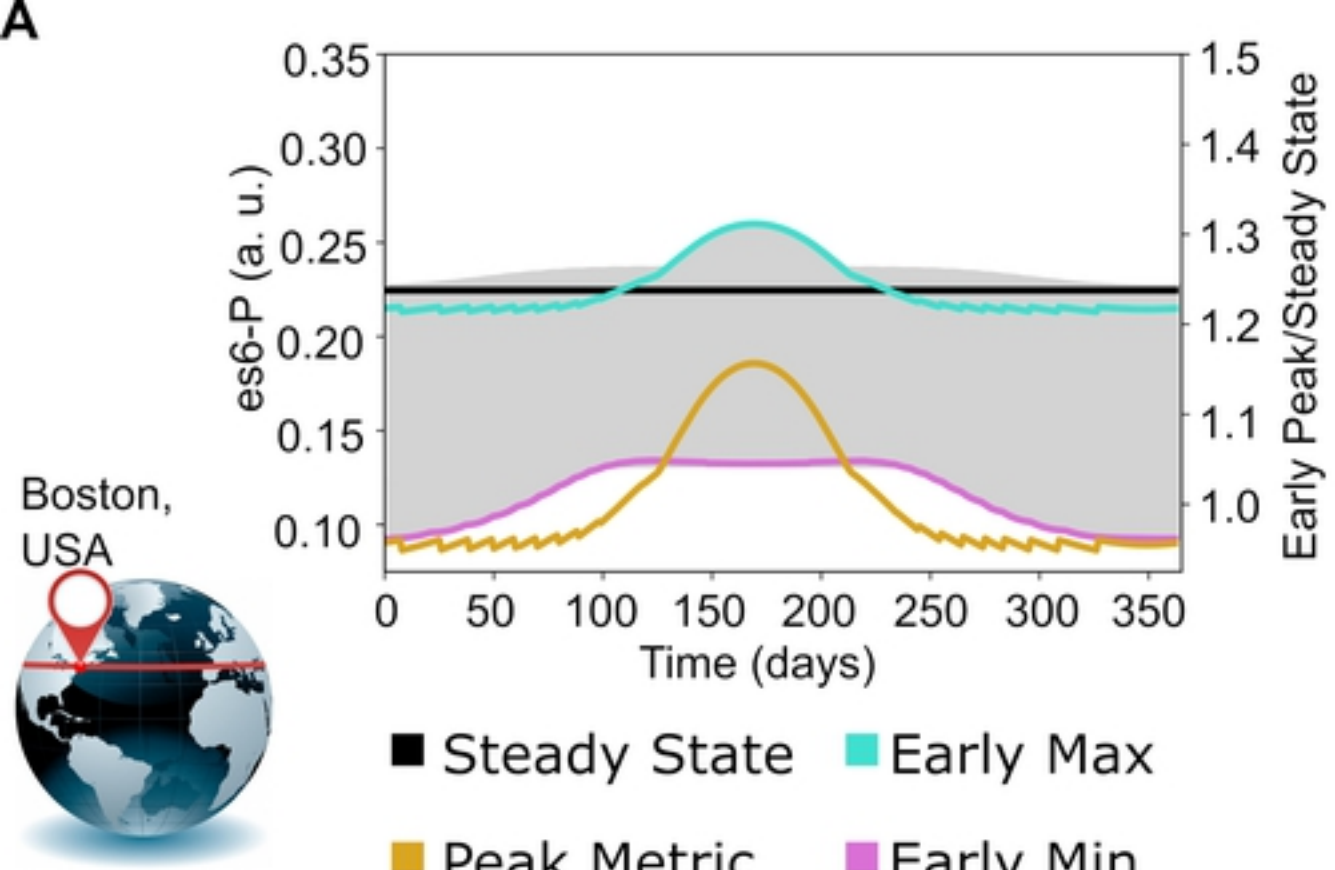
0.35
0.30
0.25
0.20
0.15
0.10
es6-P (a. u.)
1.5
1.4
1.3
1.2
1.1
1.0
Early Peak/Steady State
0
50
100
150
200
250
300
350
Time (days)
Steady State
Early Max
Peak Metric
Early Min

Boston,
USA

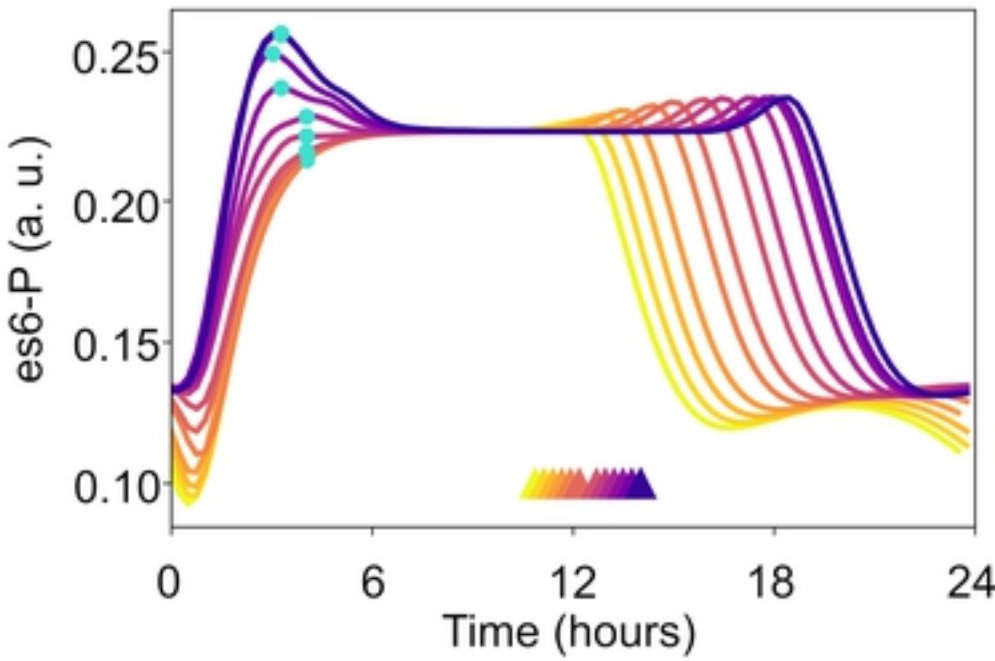
0.25
0.20
0.15
0.10
es6-P (a. u.)
0
6
12
18
24
Time (hours)
1
13
25
Week of the Year

B

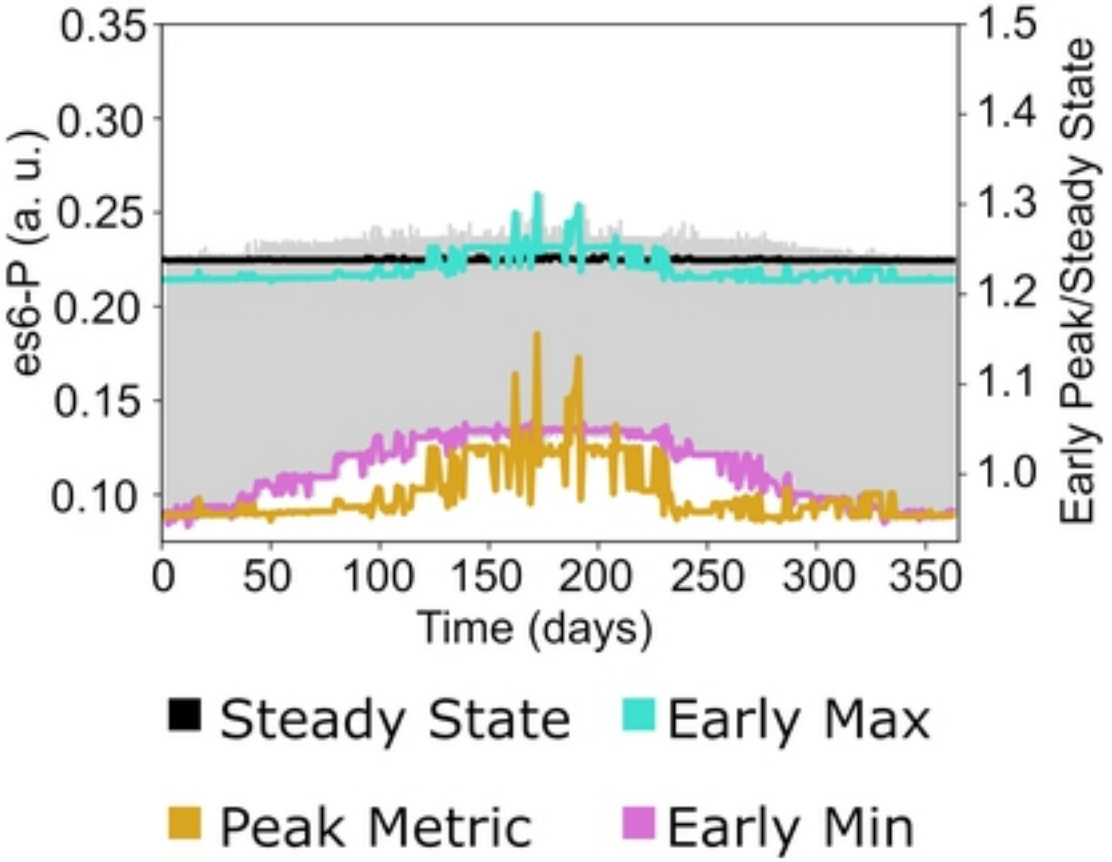
0.35
0.30
0.25
0.20
0.15
0.10
es6-P (a. u.)
1.5
1.4
1.3
1.2
1.1
1.0
Early Peak/Steady State
0
50
100
150
200
250
300
350
Time (days)
Steady State
Early Max
Peak Metric
Early Min

C

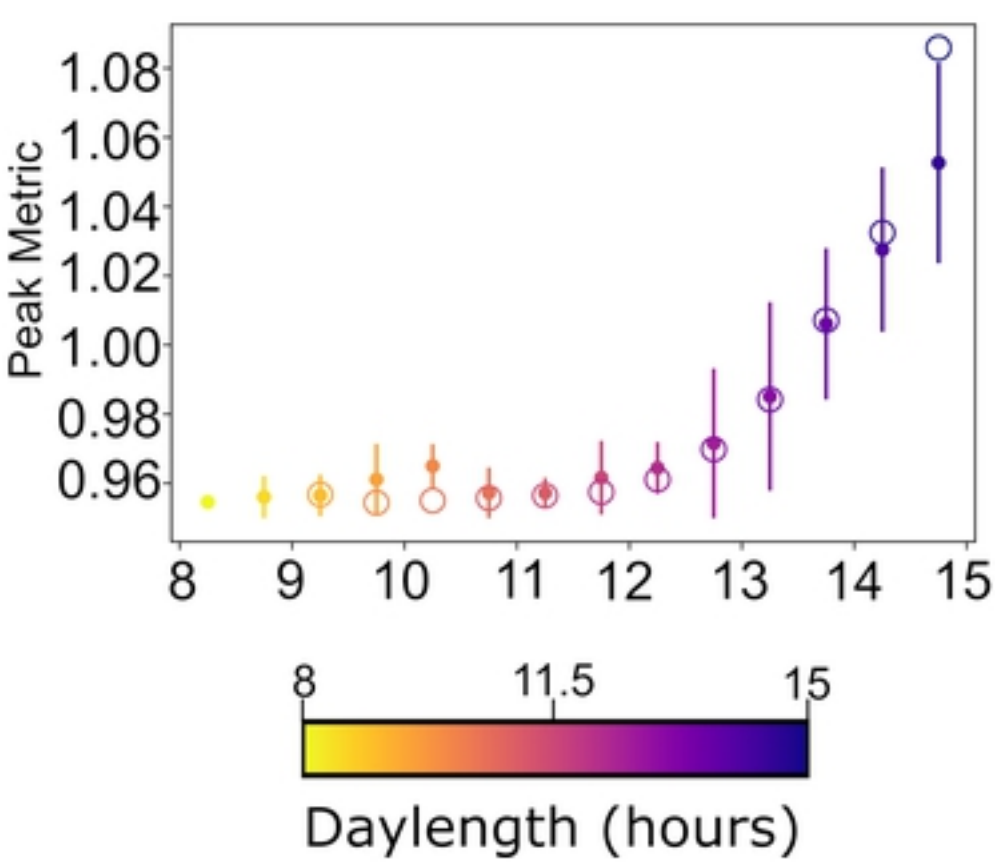
1.08
1.06
1.04
1.02
1.00
0.98
0.96
Peak Metric
8
9
10
11
12
13
14
15
8
11.5
15
Daylength (hours)

Figure 6

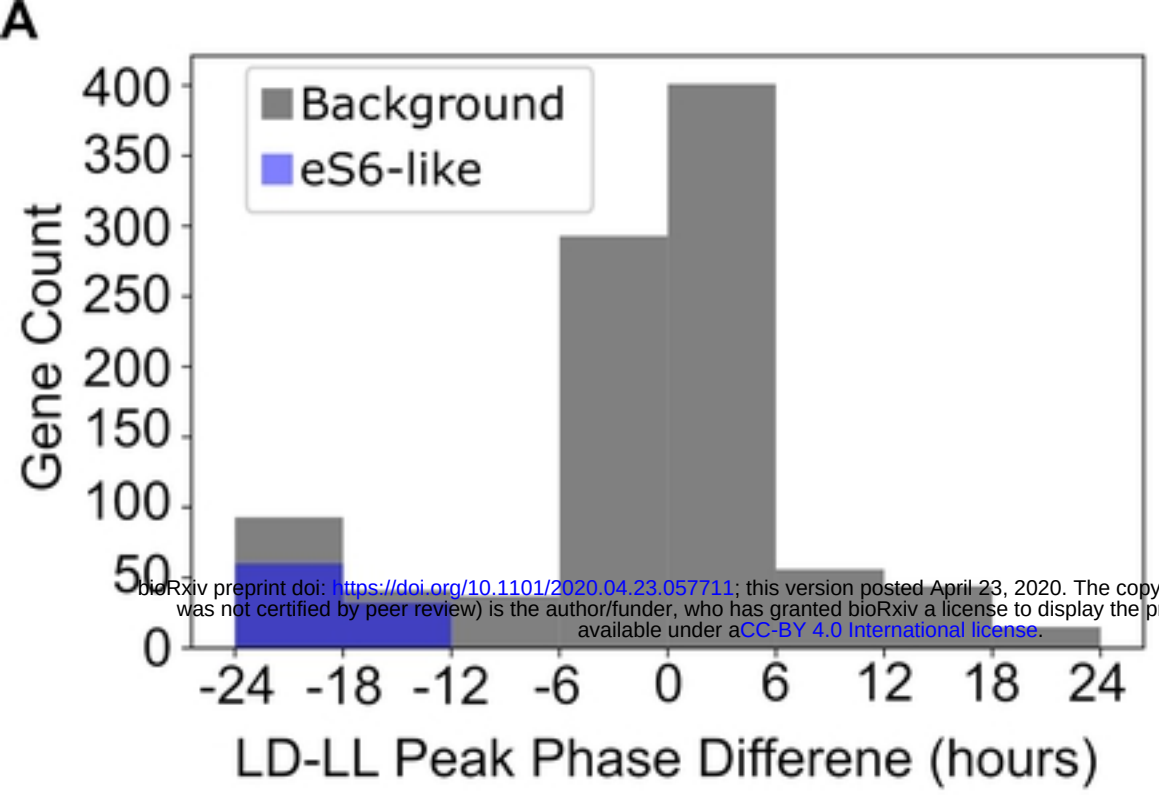

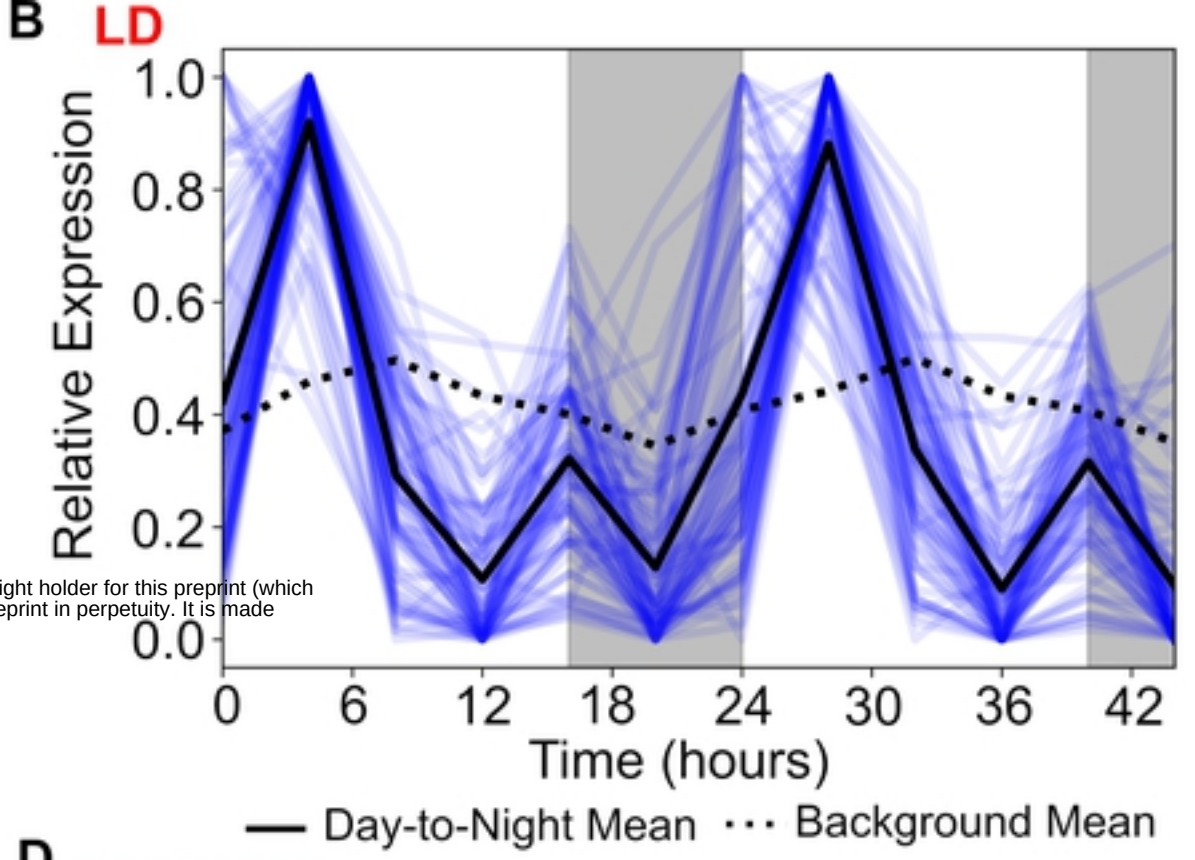

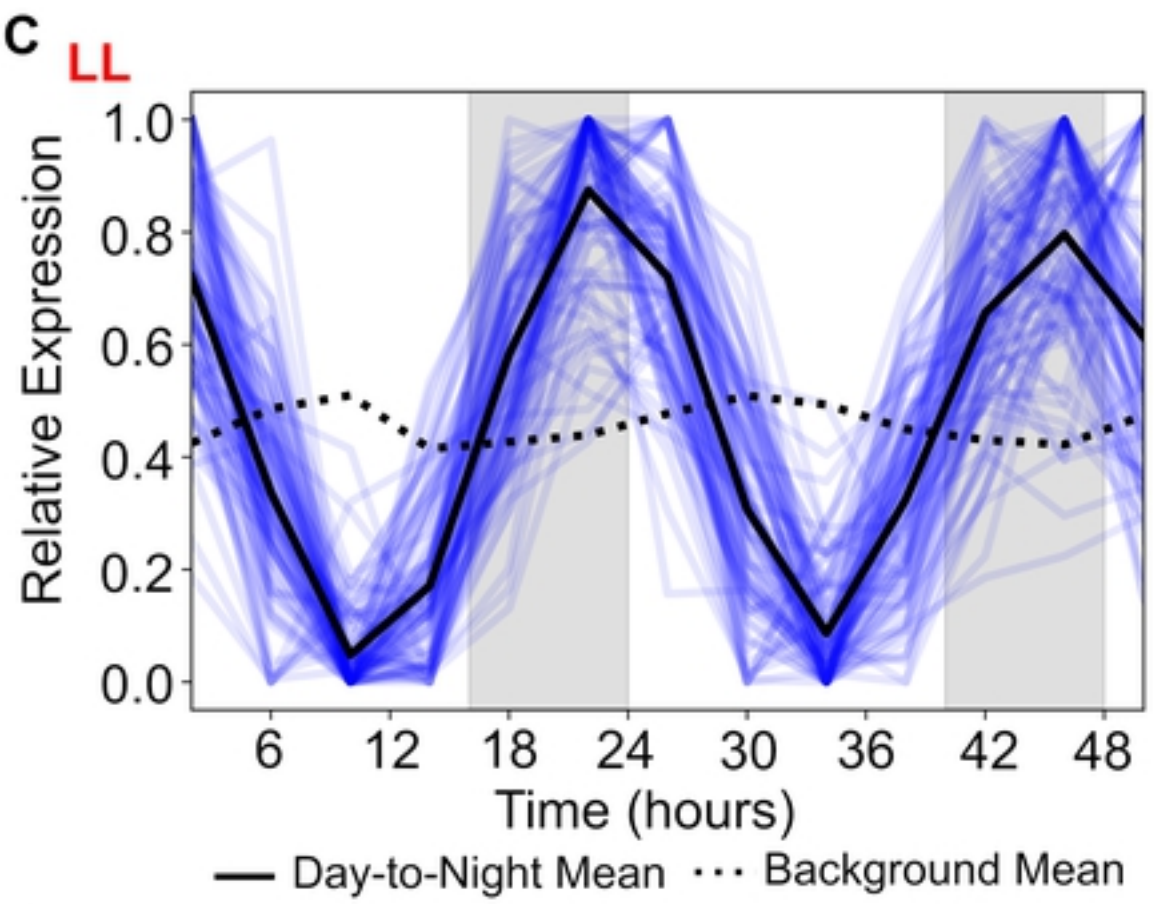

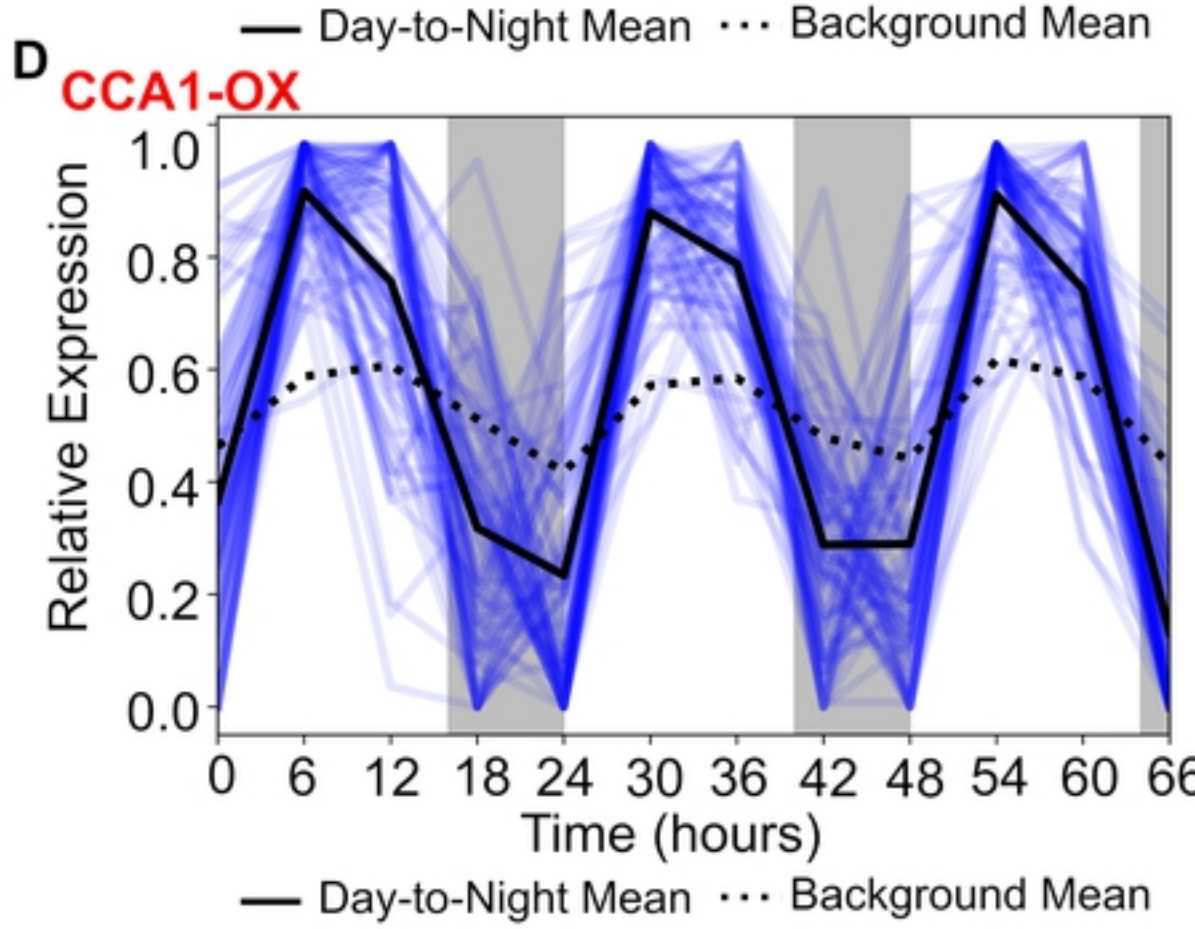

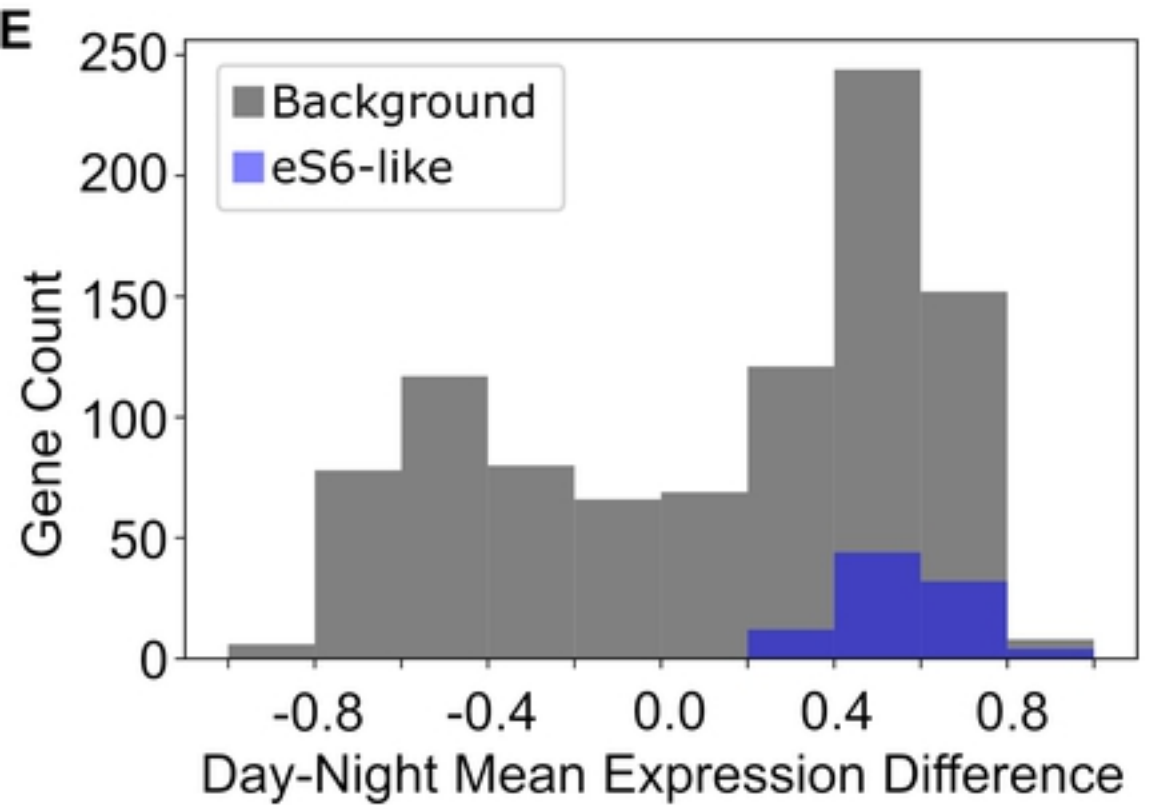

Figure 7